UNIVERSITY OF AMSTERDAM

UvA-DARE (Digital Academic Repository)

Long-lived neutral fermions at the DUNE near detector

Günther, J.Y.; de Vries, J.; Dreiner, H.K.; Wang, Z.S.; Zhou, G.

DOI
10.1007/JHEP01(2024)108

Publication date
2024

Document Version
Final published version

Published in
The Journal of High Energy Physics

License
CC BY

Link to publication

Citation for published version (APA):
Günther, J. Y., de Vries, J., Dreiner, H. K., Wang, Z. S., & Zhou, G. (2024). Long-lived neutral fermions at the DUNE near detector. *The Journal of High Energy Physics*, *2024*(1), Article 108. https://doi.org/10.1007/JHEP01(2024)108

General rights
It is not permitted to download or to forward/distribute the text or part of it without the consent of the author(s) and/or copyright holder(s), other than for strictly personal, individual use, unless the work is under an open content license (like Creative Commons).

Disclaimer/Complaints regulations
If you believe that digital publication of certain material infringes any of your rights or (privacy) interests, please let the Library know, stating your reasons. In case of a legitimate complaint, the Library will make the material inaccessible and/or remove it from the website. Please Ask the Library: https://uba.uva.nl/en/contact, or a letter to: Library of the University of Amsterdam, Secretariat, P.O. Box 19185, 1000 GD Amsterdam, The Netherlands. You will be contacted as soon as possible.

UvA-DARE is a service provided by the library of the University of Amsterdam (https://dare.uva.nl)

Download date:13 Nov 2026

Published for SISSA by Springer

Received: October 27, 2023
Accepted: December 21, 2023
Published: January 19, 2024

Long-lived neutral fermions at the DUNE near detector

Julian Y. Günther[a], **Jordy de Vries**[b,c], **Herbi K. Dreiner**[a], **Zeren Simon Wang**[d,e] and **Guanghui Zhou**[b,c,f]

[a] *Bethe Center for Theoretical Physics & Physikalisches Institut der Universität Bonn, Nußallee 12, 53115 Bonn, Germany*
[b] *Institute for Theoretical Physics Amsterdam and Delta Institute for Theoretical Physics, University of Amsterdam, Science Park 904, 1098 XH Amsterdam, The Netherlands*
[c] *Nikhef, Theory Group, Science Park 105, 1098 XG, Amsterdam, The Netherlands*
[d] *Department of Physics, National Tsing Hua University, Hsinchu 300, Taiwan*
[e] *Center for Theory and Computation, National Tsing Hua University, Hsinchu 300, Taiwan*
[f] *CAS Key Laboratory of Theoretical Physics, Institute of Theoretical Physics, Chinese Academy of Sciences, Beijing 100190, P. R. China*

E-mail: guenther@physik.uni-bonn.de, j.devries4@uva.nl, dreiner@uni-bonn.de, wzs@mx.nthu.edu.tw, zhough.uva@gmail.com

Abstract: At the Deep Underground Neutrino Experiment (DUNE), a proton beam hits a fixed target leading to large production rates of mesons. These mesons can decay and potentially provide a source of long-lived neutral fermions. Examples of such long-lived fermions are heavy neutral leptons which can mix with the standard-model active neutrinos, and the bino-like lightest neutralino in R-parity-violating supersymmetry. We show that the Standard Model Effective Field Theory extended with right-handed singlet neutrinos can simultaneously describe heavy neutral leptons and bino-like neutralinos in a unified manner. We use the effective-field-theory framework to determine the sensitivity reach of the DUNE near detector in probing various scenarios of long-lived neutral fermions.

Keywords: New Light Particles, SMEFT, Sterile or Heavy Neutrinos, Supersymmetry

ArXiv ePrint: 2310.12392

Open Access, © The Authors.
Article funded by SCOAP[3].

https://doi.org/10.1007/JHEP01(2024)108

Contents

1 Introduction **1**

2 The νSMEFT framework **2**

3 Theoretical scenarios **5**

4 Production of the neutral fermion N **7**
4.1 The minimal scenario 7
4.2 Effective operators 9

5 Decay of the neutral fermion N **9**
5.1 The minimal scenario 9
5.2 Effective operators 11

6 The DUNE experiment **12**
6.1 Monte-Carlo simulation 13
6.2 Three-dimensional detector approximation 16
6.3 Kaons at the LHC 17

7 Numerical results **18**
7.1 Minimal scenario 19
7.2 Flavor benchmarks 20
7.2.1 Flavor benchmark 1 21
7.2.2 Flavor benchmark 2 23
7.2.3 Flavor benchmark 3 25

8 Conclusions **26**

A Meson decay rate calculation **28**
A.1 Charged currents — two-body final states 28
A.2 Neutral currents — two-body final states 30
A.2.1 Heavy neutral mesons 31
A.2.2 Kaons 31
A.2.3 Light neutral mesons 32
A.3 Three body final states 33

B Phenomenological values **34**
B.1 Decay constants 35
B.2 Form factor parameterizations 35
B.2.1 Kaons: $K \to \pi$ 36
B.2.2 Charmed mesons: $D \to \pi/K$ 36
B.2.3 Charmed strange mesons: $D_s \to \eta/\eta'/K$ 37

JHEP01(2024)108

B.2.4 Bottom mesons: $B \to \pi/K/D$ and $B_s \to K/D_s$ 37
B.2.5 Bottom strange meson decays $B_s \to \eta^{(\prime)}$ 38
B.2.6 Final state vector mesons 39

C RPV derivation 39

1 Introduction

At the Deep Underground Neutrino Experiment (DUNE) [1–5], currently under construction, a wide range of physics goals will be pursued [6]. Key examples are the study of neutrino oscillations to determine the neutrino-mass ordering and the CP-violating Dirac mass mixing phase, the search for proton decay, as well as the detection of supernova neutrino bursts. In addition, DUNE will serve as a beam-dump-type experiment where a proton beam impinges on a fixed target, generating a large number of mesons. These mesons can in rare cases potentially decay into light particles that appear in broad classes of Beyond-the-Standard-Model (BSM) theories. To have avoided detection so far, such particles must interact feebly with Standard Model (SM) fields causing them to be long-lived. See refs. [7–10] for some recent reviews on long-lived particle (LLP) searches.

At DUNE, LLPs can be produced from rare meson decays, travel a macroscopic distance, and then decay in a detector far from the original fixed-target collision. While the DUNE far detector, with a distance of 1300 km from the beam target, is expected to have very limited sensitivities for LLPs, the DUNE near detector (DUNE-ND) is much closer to the beam target (574 m) and will be equipped with state-of-the-art event-reconstruction capabilities [11]. The DUNE-ND will therefore be an ideal device for detecting LLPs. Phenomenological studies on LLP detection at the DUNE-ND have already been performed in e.g. refs. [12–24].

In this work, as an example of LLPs, we focus on long-lived neutral fermions (LLNFs). A famous example is provided by heavy neutral leptons (HNLs), which are among the most sought-after candidates of LLNFs. They are SM singlets that mix with active neutrinos and can be the origin of neutrino masses [25–29]. In minimal scenarios, the HNLs only interact with SM fields through mixing with the active neutrinos. In more general scenarios, the phenomenology of the HNLs can be very different. Examples include SM extensions with an extra U(1) gauge symmetry and an associated gauge boson (Z') [30–35] or left-right symmetric models [36–39], where the HNLs interact with right-handed gauge bosons.

A very useful framework to describe these possible HNLs interactions in a unified way is the neutrino-extended standard model effective field theory (νSMEFT) [40–44]. The νSMEFT Lagrangian contains all operators involving only HNLs (assumed to be singlets under the SM gauge group) and SM fields that are invariant under Lorentz and SM gauge symmetries. The main assumption is that the only relatively light BSM particles are the HNLs and all other BSM particles are heavy degrees of freedom and can be integrated out. The νSMEFT framework can be used to efficiently describe a wide range of possible HNL scenarios and has already been used to describe HNL phenomenology at the LHC [45–47], neutrinoless double beta decay and related searches [48, 49], meson decays [50–53], B-factories such as Belle II [54, 55], as well as fixed-target experiments [45].

JHEP01(2024)108

Here, we point out that νSMEFT can describe not only the HNLs but also other SM singlets predicted in various BSM theories. For instance, the lightest neutralino in the R-parity-violating minimal supersymmetric model (MSSM) (RPV-SUSY) [56–59], if bino-like, can be very light, i.e. at the GeV-scale or even massless [60–64]. Such a light neutralino is allowed by all laboratory, as well as cosmological and observational constraints [65–72]. In these scenarios, dark matter is not comprised of the lightest neutralino [73–80], and as long as these light binos decay (which could be triggered by non-vanishing RPV operators), overclosing of the Universe is avoided [81]. Such light binos are SM singlets by definition and can be produced from meson decays through RPV operators [61, 82–84]. These decays are mediated by scalar fermions which are currently bounded from below at the TeV scale [85–91]. One can integrate out the scalar fermions and derive effective operators involving quarks, a lepton, and a light bino only [64, 92]. These operators are already included in the νSMEFT Lagrangian, if we interpret the right-handed SM singlets in the model as the light bino in the RPV-SUSY. Furthermore, if the RPV couplings are small enough, the light neutralino can easily be long-lived, leading to displaced-vertex signatures at colliders [92–94] including proposed far detectors [95–98], beam-dump experiments [61, 83, 92, 99], B-factories [100, 101], and even neutrino experiments [102].

In this paper, we investigate the sensitivity reach of the `DUNE-ND` to both HNLs and light neutralinos within the framework of the νSMEFT. The paper is organized as follows. We first introduce the νSMEFT framework in section 2, followed by section 3 listing and discussing the theoretical scenarios we study. The production and decay of the LLNFs are then discussed in sections 4 and 5, respectively. In section 6 we describe the `DUNE` experiment including the `DUNE-ND`, and elaborate on our simulation procedure. We then present our numerical results in section 7 and conclude the paper in section 8. In addition to the main text, in appendix A, we derive the relevant meson decay constants and form factors, and calculate all employed decay rates. In appendix B, we list the numerical values of the decay constants we use and the parameterization of the form factors. Finally, we provide appendix C where we present the derivation of 4-fermion effective interactions in the RPV-SUSY with the heavy sfermion fields integrated out.

2 The νSMEFT framework

Sterile neutrinos ν_R are spin-1/2, right-handed gauge-singlet fields under the SM gauge group. Without introducing additional fields, the only renormalizable interaction with SM fields is through the neutrino portal. For N_ν sterile neutrinos the renormalizable interactions are given by

$$\mathcal{L} = \mathcal{L}_{\rm SM} - \left[\epsilon_{ab}(L_a)_i^T \tilde{H}_b (Y_\nu)_{ij} \nu_{Rj} + \frac{1}{2}\bar{\nu}^c_{Ri}\bar{M}_{Rij}\nu_{Rj} + \text{h.c.}\right], \tag{2.1}$$

where $\mathcal{L}_{\rm SM}$ is the SM Lagrangian. H is the SM complex scalar Higgs SU(2)$_L$ doublet, which in the unitary gauge becomes

$$H = \frac{v}{\sqrt{2}}\begin{pmatrix} 0 \\ 1 + \frac{h}{v} \end{pmatrix}, \tag{2.2}$$

JHEP01(2024)108

in terms of the Higgs boson h and the Higgs vacuum expectation value $v \simeq 246\,\text{GeV}$. In the Yukawa coupling we use $\tilde{H} = i\tau_2 H^*$. $(L_a)_i$ denote the SM $\text{SU}(2)_L$ lepton doublet fields, with $\text{SU}(2)_L$ gauge indices $a, b \in \{1, 2\}$ for the fundamental representation, and generation indices $i \in \{1, 2, 3\}$. ϵ_{kl} denotes the anti-symmetric tensor with $\epsilon_{12} = +1$. ν_{Rj} are the sterile neutrino fields with generation indices $j \in \{1, 2, \ldots, N_\nu\}$. Y_ν is then a $3 \times N_\nu$ matrix consisting of Yukawa couplings and $\bar{M}_R$ is a complex symmetric Majorana mass matrix. ψ^c is the charge conjugate field of ψ, where we define $\psi^c \equiv C\bar{\psi}^T$, with the charge conjugation matrix $C = -i\gamma^2\gamma^0$. For chiral spinors $\psi_{L,R} = P_{L,R}\psi$ with the projection operators $P_{L,R} = (1 \mp \gamma_5)/2$, we define $\psi^c_{L,R} \equiv (\psi_{L,R})^c \equiv C\overline{\psi_{L,R}}^T = P_{R,L}\psi^c$.

The Lagrangian in eq. (2.1) corresponds to a minimal model where sterile neutrinos only interact through mixing with left-handed active neutrinos. It is not unlikely that sterile neutrinos only appear sterile, but actually have additional interactions that are decoupled at low energies. A possible scenario would be left-right symmetric models where sterile neutrinos are charged under non-SM gauge symmetries and interact through the exchange of right-handed gauge bosons. Assuming that such interactions arise from the exchange of particles with masses well above the electroweak (EW) scale, at lower energies they can be described with the νSMEFT Lagrangian

$$\mathcal{L}_{\nu\text{SMEFT}} = \mathcal{L} + \sum_{d>4} \sum_i C_i^{(d)} \mathcal{O}_i^{(d)} \,. \tag{2.3}$$

Here, $\mathcal{O}_i^{(d)}$ is a dimension d operator consisting just of SM fields and ν_{Ri}, and $C_i^{(d)}$ are Wilson coefficients that scale as $(\Lambda)^{4-d}$. The experiments we consider involve energy scales well below the electroweak scale, and the νSMEFT Lagrangian can be matched to an effective field theory (EFT) where heavy degrees of freedom (e.g. Higgs, top, $W^\pm$, Z, and potentially some sterile neutrinos) are integrated out. The resulting EFT satisfies $\text{SU}(3)_c \times \text{U}(1)_{\text{em}}$ gauge symmetry. We give more details below.

For simplicity, we consider only one sterile neutrino ($N_\nu = 1$), as including more sterile neutrinos does not significantly impact the observables under consideration. With only one sterile neutrino, the dimension-5 νSMEFT operators contribute to the Majorana masses of ν_L and ν_R fields after electroweak symmetry breaking. They can be absorbed into the active and sterile neutrino masses and we do not consider them here.

At the level of the dimension-6 operators, we restrict ourselves to the operators involving only one sterile neutrino field; they are shown in table 1. Not all operators are relevant for our purposes. The $\mathcal{O}_{L\nu H}$ operator can be effectively absorbed in the dimension-4 $L\nu H$ interaction in eq. (2.1), up to terms with explicit Higgs bosons, which play no role in our analysis. The dipole operators $\mathcal{O}_{\nu W}^{(6)}$ and $\mathcal{O}_{\nu B}^{(6)}$ are strongly constrained by searches for neutrino dipole moments [103, 104] and mainly lead to displaced-vertex signatures of a single photon which are relevant only for a limited set of the proposed experiments [105–107]. We therefore only keep the $O_{H\nu e}$ operator and the five four-fermion operators.

We apply one-loop QCD anomalous dimensions to evolve these operators from Λ to the electroweak scale v, except $\mathcal{O}_{H\nu e}^{(6)}$, which does not evolve under the one-loop QCD. For the remaining operators, we find [48]

$$\frac{dC_{Qu\nu L}^{(6)}}{d\ln\mu} = \left(\frac{\alpha_s}{4\pi}\right)\gamma_S\, C_{Qu\nu L}^{(6)}\,, \qquad \frac{dC_S^{(6)}}{d\ln\mu} = \left(\frac{\alpha_s}{4\pi}\right)\gamma_S\, C_S^{(6)}\,, \qquad \frac{dC_T^{(6)}}{d\ln\mu} = \left(\frac{\alpha_s}{4\pi}\right)\gamma_T\, C_T^{(6)}\,, \tag{2.4}$$

JHEP01(2024)108

	$\psi^2 H^3$		ψ^4
$\mathcal{O}_{L\nu H}$	$(\bar{L}\nu_R)\tilde{H}(H^\dagger H)$	$\mathcal{O}_{du\nu e}$	$(\bar{d}_R\gamma^\mu u_R)(\bar{\nu}_R\gamma_\mu e)$
	$\psi^2 H^2 D$	$\mathcal{O}_{Qu\nu L}$	$(\bar{Q}u_R)(\bar{\nu}_R L)$
$\mathcal{O}_{H\nu e}$	$(\bar{\nu}_R\gamma^\mu e_R)(\tilde{H}^\dagger iD_\mu H)$	$\mathcal{O}_{L\nu Qd}$	$(\bar{L}\nu_R)\epsilon(\bar{Q}d_R)$
	$\psi^2 HF$	$\mathcal{O}_{LdQ\nu}$	$(\bar{L}d_R)\epsilon(\bar{Q}\nu_R)$
$\mathcal{O}_{\nu W}$	$(\bar{L}\sigma_{\mu\nu}\nu_R)\tau^I\tilde{H}W^{I\mu\nu}$	$\mathcal{O}_{L\nu Le}$	$(\bar{L}\nu_R)\epsilon(\bar{L}e_R)$
$\mathcal{O}_{\nu B}$	$(\bar{L}\sigma_{\mu\nu}\nu_R)\tilde{H}B^{\mu\nu}$		

Table 1. Dimension-6 operators that involve one ν_R field. Each fermion field has a generation index, except ν_R, which, if necessary, are explicitly indicated. For example, $\mathcal{O}^{211}_{du\nu e}$ refers to the operator $(\bar{s_R}\gamma^\mu u_R)(\bar{\nu}_R\gamma_\mu e_R)$. We work in the basis where all the SM fields are mass eigenstates, except the left-handed down-type quarks d^i_L, for which we have $d^i_L = V^{ij}d^{j,\text{mass}}_L$ with V being the CKM matrix and $d^{j,\text{mass}}_L$ the down-like quark mass eigenstates.

where $\gamma_S = -6C_F$ and $\gamma_T = 2C_F$, with $C_F = (N_c^2-1)/(2N_c)$ and $N_c = 3$, the number of colors. $C_S^{(6)}$ and $C_T^{(6)}$ are defined as

$$C_S^{(6)} = -\frac{1}{2}C^{(6)}_{LdQ\nu} + C^{(6)}_{L\nu Qd}\,, \qquad C_T^{(6)} = -\frac{1}{8}C^{(6)}_{LdQ\nu}\,. \tag{2.5}$$

At the electroweak scale we integrate out the heavy SM fields and we match to the neutrino-extended low-energy EFT (νLEFT). For our purpose, the most important operators are Fermi-like charged-current operators

$$\begin{aligned}\mathcal{L}^{(6)}_{CC} = \frac{2G_F}{\sqrt{2}}\sum_{i,j,k}\Big\{&\bar{u}^i_L\gamma^\mu d^j_L\left[\bar{e}^k_L\gamma_\mu(-2V_{ij})\,\nu^k_L + \bar{e}^k_R\gamma_\mu c^{CC1}_{\text{VLR},ijk}\,\nu_R\right] + \bar{u}^i_R\gamma^\mu d^j_R\,\bar{e}^k_R\,\gamma_\mu c^{CC}_{\text{VRR},ijk}\,\nu_R\\ &+ \bar{u}^i_L d^j_R\,\bar{e}^k_L\,c^{CC}_{\text{SRR},ijk}\nu_R + \bar{u}^i_R d^j_L\,\bar{e}^k_L\,c^{CC}_{\text{SLR},ijk}\nu_R + \bar{u}^i_L\sigma^{\mu\nu}d^j_R\,\bar{e}^k_L\sigma_{\mu\nu}c^{CC}_{\text{T},ijk}\,\nu_R\\ &+ \bar{\nu}^i_L\gamma^\mu e^j_L\,\bar{e}^k_R\gamma_\mu c^{CC2}_{\text{VLR},ijk}\nu_R + \text{h.c.}\Big\} - \frac{4G_F}{\sqrt{2}}\sum_{i,j}\bar{\nu}^i_L\gamma^\mu e^i_L\bar{e}^j_L\gamma_\mu\nu^j_L,\end{aligned} \tag{2.6}$$

in terms of chiral charged up-type quarks, $u^i_{L,R}$, down-type quarks $d^i_{L,R}$, charged leptons $e^i_{L,R}$, and left-handed neutrinos ν^i_L, where $i = \{1,2,3\}$ denote generation indices.

For the neutral-current interactions, we obtain[1]

$$\begin{aligned}\mathcal{L}^{(6)}_{\text{NC}} = \frac{-4G_F}{\sqrt{2}}\sum_{i,j}\bar{\nu}^i_L\gamma^\mu\nu^i_L\Big\{&\bar{e}^j_L\gamma_\mu\left(-\frac{1}{2}+\sin^2\theta_W\right)e^j_L + \bar{e}^j_R\gamma_\mu(\sin^2\theta_W)e^j_R\\ &+\bar{u}^j_L\gamma^\mu\left(\frac{1}{2}-\frac{2}{3}\sin^2\theta_W\right)u^j_L + \bar{u}^j_R\gamma_\mu\left(-\frac{2}{3}\sin^2\theta_W\right)u^j_R\\ &+\bar{d}^j_L\gamma^\mu\left(-\frac{1}{2}+\frac{1}{3}\sin^2\theta_W\right)d^j_L + \bar{d}^j_R\gamma_\mu\left(\frac{1}{3}\sin^2\theta_W\right)d^j_R + \frac{1}{4}(2-\delta_{ij})\bar{\nu}^j_L\gamma^\mu\nu^j_L\Big\}\\ &+\frac{2G_F}{\sqrt{2}}\sum_{i,j,k}\Big\{\bar{u}^i_R u^j_L\bar{\nu}^k_L c^{NC}_{\text{SLR},ijk}\nu_R + \bar{d}^i_L d^j_R\bar{\nu}^k_L c^{NC}_{\text{SRR},ijk}\nu_R + \bar{d}^i_L\sigma^{\mu\nu}d^j_R\bar{\nu}^k_L\sigma_{\mu\nu}c^{NC}_{\text{T},ijk}\nu_R + \text{h.c.}\Big\},\end{aligned} \tag{2.7}$$

with θ_W being the electroweak mixing angle.

[1] Except for the SM weak interactions, no neutral (axial-)vector-like currents are present in the $\mathcal{L}_{\nu\text{LEFT}}$. None of the dimension-6 operators introduced in table 1 include such currents, neither directly nor after rearranging the currents with Fierz-identities.

JHEP01(2024)108

The dimensionless Wilson coefficients, c, are then obtained from a tree-level matching calculation to the νSMEFT Lagrangian at the electroweak scale [48, 54]. For charged currents we use

$$
\begin{aligned}
c^{CC1}_{\mathrm{VLR},ijk} &= \left[-v^2 C_{H\nu e,k}\right]^\dagger V_{ij}\,, & c^{CC2}_{\mathrm{VLR},ijk} &= \left[-v^2 C_{H\nu e,k}\right]^\dagger \delta_{ij}\,,\\
c^{CC}_{\mathrm{VRR},ijk} &= v^2\left(C_{du\nu e,jik}\right)^\dagger\,, & c^{CC}_{\mathrm{T},ijk} &= \frac{v^2}{8} C_{LdQ\nu,kji}\,,\\
c^{CC}_{\mathrm{SRR},ijk} &= -v^2 C_{L\nu Qd,kij} + \frac{v^2}{2} C_{LdQ\nu,kji}\,, & c^{CC}_{\mathrm{SLR},ijk} &= v^2\left(C_{Qu\nu L,lik}\right)^\dagger V_{lj}\,,
\end{aligned}
\tag{2.8}
$$

where repeated flavor indices are summed over. For neutral currents, we find

$$
\begin{aligned}
c^{NC}_{\mathrm{SLR},ijk} &= v^2\left(C_{Qu\nu L,jik}\right)^\dagger\,, & c^{NC}_{\mathrm{SRR},ijk} &= v^2 C_{L\nu Qd,klj} V^*_{li} - \frac{v^2}{2} C_{LdQ\nu,kjl} V^*_{li}\,,\\
c^{NC}_{\mathrm{T},ijk} &= -\frac{v^2}{8} C_{LdQ\nu,kjl} V^*_{li}\,.
\end{aligned}
\tag{2.9}
$$

Finally, we evolve both charged- and neutral-current operators from the EW scale down to the QCD scale $\Lambda_{\mathrm{QCD}} \simeq 1\,\mathrm{GeV}$, using the one-loop QCD running. The vector-type interactions do not evolve. Only the scalar- and tensor-type operators in eqs. (2.8) and (2.9) evolve analogously to eq. (2.4). This evolution leads to an enhancement of the scalar-type interactions of roughly 60%, while the tensor-type ones are suppressed by 15% [108].

3 Theoretical scenarios

Instead of an exhaustive analysis of the very large parameter space of the νSMEFT, we consider four representative scenarios in which a single long-lived neutral fermion N is kinematically relevant:

1. We first study the minimal case, where we turn off all higher-dimensional operators and the sterile neutrino only interacts with the SM fields through the SM weak interaction after mixing. Active neutrinos ν^k_L are related to neutrino mass eigenstates ν_i through

$$
\nu^k_L = U_{kl}\nu_l, \tag{3.1}
$$

   where $l = 1,2,3,4$ and $k = e,\mu,\tau$. We focus on the mixing angle $U_{e4} \neq 0$ for the sterile neutrino. We keep U_{e4} as a free parameter (considering the stringent bounds on U_{e4} we can freely interchange ν_R and ν_4). The first interaction in eq. (2.6) then includes the term

$$
\mathcal{L}^{(6)}_{CC} = \frac{2G_F}{\sqrt{2}} \sum_{i,j} c^{CC}_{\mathrm{VLL},ij} (\bar{u}^i_L \gamma^\mu d^j_L)(\bar{e}_L \gamma_\mu \nu_R) \tag{3.2}
$$

   where we introduced the coefficient $c^{CC}_{\mathrm{VLL},ij} = -2V_{ij}U_{e4}$.

2. In the second scenario, we introduce leptoquarks, which are hypothetical scalar or vector particles that allow for the transition of leptons into quarks and vice versa [109]. A multitude of leptoquark representations are possible (for an extensive review, see

JHEP01(2024)108

ref. [110]). As an example, we focus on matter interacting with the leptoquark representation $\tilde{R}_2$ with SM gauge group $(\mathrm{SU}(3)_C, \mathrm{SU}(2)_L, \mathrm{U}(1)_Y)$ transformation properties $(\mathbf{3}, \mathbf{2}, 1/6)$. This leads to the Lagrangian

$$\mathcal{L}_{\mathrm{LQ}} = -y^{RL}_{jk}\bar{d}_{Rj}\tilde{R}^a_2\epsilon^{ab}L^b_{Lk} + y^{\overline{LR}}_i\bar{Q}^a_{Li}\tilde{R}^a_2\nu_R + \mathrm{h.c.}\,, \tag{3.3}$$

where a, b are $SU_L(2)$ gauge indices, i, j, k are flavor indices, and y^{RL}_{jk} and $y^{\overline{LR}}_i$ are complex Yukawa coupling matrices. The mass of the leptoquark is restricted by direct and indirect searches [111] to be $m_{\mathrm{LQ}} > \mathcal{O}(1\,\mathrm{TeV})$. Integrating out the leptoquark leads to the matching relation

$$C_{LdQ\nu,kji} = \frac{1}{m^2_{\mathrm{LQ}}}\, y^{\overline{LR}}_i\, y^{RL*}_{jk}\,. \tag{3.4}$$

Below the EW scale, we fix the lepton generational index to electrons $k = e$ and match the interactions to νLEFT with

$$\begin{aligned} c^{CC}_{\mathrm{VLL},ij} &= -2V_{ij}U_{e4}\,, \\ c^{CC}_{\mathrm{SRR},ije} &= 4c^{CC}_{\mathrm{T},ije} = \frac{v^2}{2}\frac{1}{m^2_{\mathrm{LQ}}} y^{\overline{LR}}_i (y^{RL}_{je})^*\,, \\ c^{NC}_{\mathrm{SRR},ije} &= 4c^{NC}_{\mathrm{T},ije} = -V^*_{li}\, c^{CC}_{\mathrm{SRR},lje}\,. \end{aligned} \tag{3.5}$$

3. In left-right symmetric models the SM gauge group is extended by an $\mathrm{SU}(2)_R$ and sterile neutrinos arise naturally. This introduces new gauge fields which interact with right-handed neutrinos and which can mix with SM $\mathrm{SU}(2)_L$ gauge bosons after spontaneous symmetry breaking. LHC and low-energy precision experiments constrain the extra gauge bosons to be heavier than several TeV [112, 113]. After integrating them out, we again induce contributions to higher-dimensional νSMEFT operators. Instead of performing a detailed analysis, we consider c^{CC1}_{VLR} to be the only non-zero Wilson coefficient in combination with minimal mixing and fix $k = e$. We summarize the non-vanishing couplings here:

$$\begin{aligned} c^{CC}_{\mathrm{VLL},ij} &= -2V_{ij}U_{e4}\,, \\ c^{CC1}_{\mathrm{VLR},ije} &\neq 0\,, \end{aligned} \tag{3.6}$$

and set $c^{CC1}_{\mathrm{VLR},ije} > 0$ for concreteness. A more complete analysis of displaced-vertex searches for left-right symmetric models at `DUNE` and elsewhere is work in progress (see also ref. [114]).

4. The νSMEFT framework can also be used to match other frameworks involving a SM-singlet fermion to the EFT, which is not related to neutrino physics. That is, our framework is *not* restricted to neutrino physics. One such framework is RPV-SUSY with the lightest neutralino being very light and hence dominantly bino-like. The bino couples via $\mathrm{U}(1)_Y$ gauge interactions to pairs of either squarks and quarks or sleptons and leptons. The virtual sfermions couple here via a non-zero RPV-operator

JHEP01(2024)108

$\lambda'_{ijk} L_i Q_j \bar{D}_k$ to SM quarks and leptons. Integrating out the heavy sfermion fields (see appendix C for details) and applying $k = e$, we obtain the effective interactions[2]

$$
\begin{aligned}
c^{CC}_{\mathrm{VLL},ij} &= 0\,, \\
c^{CC}_{\mathrm{SRR},ije} &= -36 c^{CC}_{\mathrm{T},ije} = \frac{3}{4}\frac{g'}{G_F}\frac{(\lambda'_{eij})^*}{m^2_{\mathrm{SUSY}}}\,, \\
c^{NC}_{\mathrm{SRR},ije} &= -36 c^{NC}_{\mathrm{T},ije} = -c^{CC}_{\mathrm{SRR},lje} V^*_{li}\,,
\end{aligned}
\tag{3.7}
$$

where g' is the $\mathrm{U}(1)_Y$ coupling constant and m_{SUSY} is the sfermion mass-scale.

4 Production of the neutral fermion N

In this section, we discuss the production of Majorana fermions, N, through meson decays.[3] The branching ratios into N are small for mesons with a relatively short lifetime (such as vector mesons, and η and η' mesons) and we neglect their contributions. Further, the production rate of the B_c mesons at DUNE is rather small, so we also ignore these contributions. Finally, we do not include the production of N in pion decays because our simulation tool of choice, PYTHIA8, does not predict forward pion-production very well (see also ref. [118] for a recent work on tuning PYTHIA8 for the forward physics spectra). This essentially implies that our analysis is only reliable for Majorana fermion masses above the pion mass threshold. To summarize, we consider production of a single N in the decays of pseudoscalar mesons: kaons ($K^{\pm}$, $K_{L/S}$), D-mesons ($D^{\pm}$, D^0, $D_s^{\pm}$), and B-mesons ($B^{\pm}$, B^0, B_s^0).

4.1 The minimal scenario

In the minimal scenario, we do not consider νSMEFT operators. The N can only interact with the SM fields through mixing with the active neutrinos. The only non-zero coupling is

$$
c^{CC}_{\mathrm{VLL},ij} = -2 V_{ij} U_{e4}, \tag{4.1}
$$

where i and j are the generational indices of up- and down-type generation, respectively. Such a coupling induces leptonic and semi-leptonic decays of a meson $M^{(\pm)}$ into an N, an electron, and possibly an accompanying lighter meson M':

$$
M^{\pm} \to N + e^{\pm}\,, \tag{4.2}
$$

$$
M \to N + e^{\pm} + M'\,. \tag{4.3}
$$

Depending on the mass of N and the contributing mesons M and M', both leptonic and semi-leptonic modes should be taken into account when evaluating the number of LLNF. The N-production rate depends not only on the meson decay branching ratio, but also the number of initial mesons N_M at a given experimental facility. Hence, a branching ratio for a decay mode $M_1 \to N + X_1$ smaller than that for another mode $M_2 \to N + X_2$ could still contribute significantly to the total number of N's produced.

[2] We neglect here the potential mixing between the neutralinos and the neutrinos obtained for example via bilinear R-parity breaking as this dominantly involves the higgsino component of the neutralino [115].

[3] The production of N in the GeV mass range from the decays of Higgs-, W-, and Z-bosons or via the direct production at the target is sub-dominant and hence not considered [9, 116, 117].

JHEP01(2024)108

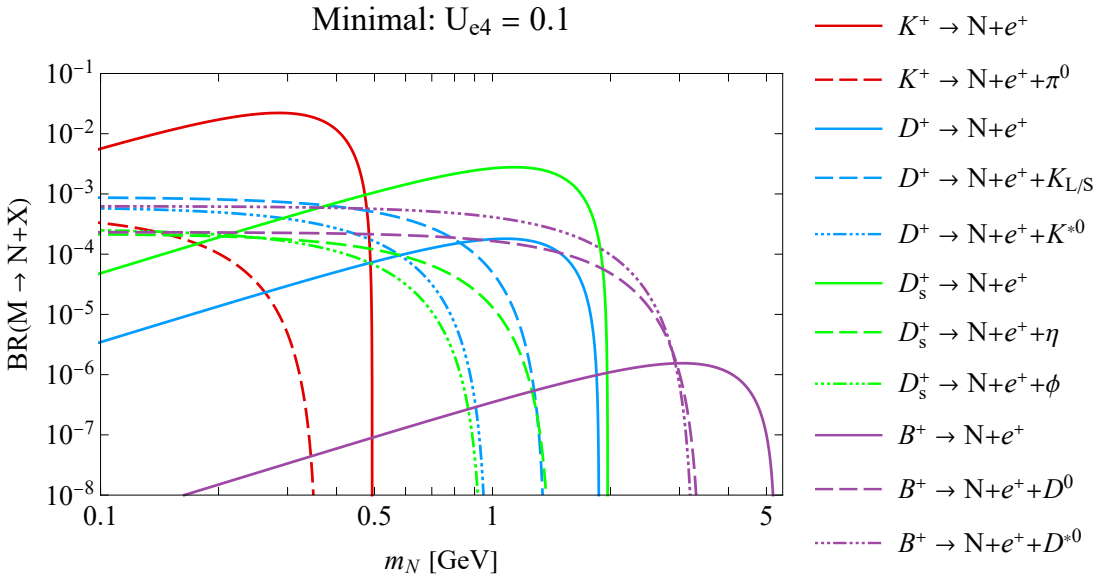

Figure 1. Branching ratios for a subset of dominant production modes (see table 2) of a $\mathcal{O}$(GeV) LLNF N *only* mixing with the electron neutrino ν_e. No higher-dimensional effective operator is switched on. The mixing parameter U_{e4} is set to 0.1.

V_{ij}	M	M'	$M^{*\prime}$	V_{ij}	M	M'	$M^{*\prime}$	V_{ij}	M	M'	$M^{*\prime}$
V_{us}	$K^\pm$	π^0		V_{ub}	$B^\pm$	π^0	ρ^0				
	$K_{L/S}$	$\pi^\mp$			B^0	$\pi^\mp$	$\rho^\mp$				
					B_s^0	$K_{L/S}$	K^{*0}				
V_{cd}	$D^\pm$	π^0	ρ^0	V_{cs}	$D^\pm$	$K_{L/S}$	K^{*0}	V_{cb}	$B^\pm$	D^0	D^{*0}
	D^0	$\pi^\mp$	$\rho^\mp$		D^0	$K^\mp$	$K^{*\mp}$		B^0	$D^\mp$	$D^{*\mp}$
	$D_s^\pm$	$K_{L/S}$	K^{*0}		$D_s^\pm$	$\eta^{(\prime)}$	ϕ		B_s^0	$D_s^\mp$	$D_s^{*\mp}$

Table 2. All included N production modes of the form $M \to N + e^\pm + M^{(*)\prime}$ in the minimal scenario. We give also the responsible CKM matrix element V_{ij} for the meson decay.

For the leptonic modes as given in eq. (4.2), we include the following $M^\pm$'s via CKM element V_{ij}: $K^\pm$ (V_{us}), $D^\pm$ (V_{cd}), $D_s^\pm$ (V_{cs}), and $B^\pm$ (V_{ub}). The included semi-leptonic modes are summarized in table 2. We have considered only the lowest excited states of e.g. kaons in the decay channels of the bottom mesons. In principle multiple higher resonances exist and could give non-negligible contributions (see, for instance, ref. [119] where it is shown that these channels are relevant for the production of a light scalar from B-meson decays that mixes with the SM Higgs boson at the LHC). These contributions only affect our results marginally because our production modes are dominated by the two-body decays of the B-mesons. We have therefore not included these excited states in our simulations. The same conclusion holds for the effective-operator scenarios as well.

The branching ratios for a subset of these decay modes are depicted in figure 1 for a minimal mixing $U_{e4} = 0.1$ (see appendix A for explicit calculations). Our results agree well with previous computations [20, 45, 120].

JHEP01(2024)108

4.2 Effective operators

In Scenarios 2–4, cf. section 3, we turn on specific EFT-operators. Depending on the quark-flavor indices of the operators, different leptonic and semi-leptonic N production modes are allowed. The relevant branching ratios have already been calculated for D- and B-meson decays via the charged currents of eq. (2.6) [45]. However, in ref. [45], the branching ratios for kaon decays were not included and neutral currents, cf. eq. (2.7), present in the leptoquark and RPV scenarios, were not taken into account.[4] In addition to the decay modes given in eqs. (4.2)–(4.3), we here consider

$$M^0 \to N + \nu_e \,, \tag{4.4}$$

$$M \to N + \nu_e + M' \,. \tag{4.5}$$

For several νSMEFT operators, neutral decays involving different quark flavors are possible because of the insertion of the CKM matrix in the matching expressions in eq. (2.9). However, some of these are suppressed by small CKM entries.

We select several flavor benchmarks for each theoretical scenario and stress that N can be either the HNL or another particle such as the light bino in RPV-SUSY. We have fixed the lepton index $k = e$ so that we only consider electrons and electron neutrinos, as the phenomenology for muons is very similar, while τ leptons are too heavy for DUNE. The production of B-mesons at DUNE is comparatively low and we therefore do not consider flavor couplings in which the production of N is mainly mediated by B-mesons. The possible up- and down-type generational quark indices ij for the charged currents are set to 11, 12 and 21. Including the related neutral couplings with quark indices lj suppressed by $|V_{il}|^2$, the possible meson decay modes for kaons, charm, and bottom mesons are listed in table 3.

For details of the associated decay rates we refer to appendix A. Neglecting possible interference arising from a non-zero U_{e4}, a subset of the branching ratios of these production modes are depicted in figure 2, as a function of the mass of N, where we set the values of the relevant dimensionless Wilson coefficients to be 0.01. The upper left plot is for the left-right symmetric model-like scenario with the Wilson coefficients $c^{CC1}_{\mathrm{VLR},12e}$ and $c^{CC1}_{\mathrm{VLR},21e}$ leading to kaon and charm-meson decays, respectively. The other three plots are for the leptoquark scenario for three different flavor generation indices. The number of decay modes in the leptoquark scenario is greater than in the left-right model-like scenario, because of the numerous neutral modes available (suppressed by the CKM matrix elements though). The RPV-SUSY scenario plots are not presented here for the reason given below. From the relations between the Wilson coefficients and the UV-complete model parameters, *cf.* eq. (3.5) and eq. (3.7), we observe that the leptoquark and RPV scenarios with $U_{e4} = 0$ *only* differ in the magnitude of the tensor currents, and the contributions from these tensor currents to the depicted decays are minor. As a result, the branching ratios of the RPV scenario are almost identical to those of the leptoquark scenario.

5 Decay of the neutral fermion N

5.1 The minimal scenario

The decay rates of an N interacting with the SM fields through minimal mixing have been calculated extensively; see e.g. refs. [20, 45, 120–124]. Here, we mainly follow ref. [45]. The

[4] See also ref. [53] for a recent work on kaon decays to the HNLs in the νSMEFT and νLEFT.

JHEP01(2024)108

ij	$M \to N + e^\pm$	$M \to N + e^\pm + M^{(*)\prime}$			V_{il}	$M \to N + \nu_e$	$M \to N + \nu_e + M^{(*)\prime}$		
	M	M	M'	$M^{*\prime}$		M	M	M'	$M^{*\prime}$
11					V_{us}	$K_{L/S}$	$K^\pm$	$\pi^\pm$	
							$K_{L/S}$	π^0	
					V_{ub}	B^0	$B^\pm$	$\pi^\pm$	$\rho^\pm$
							B^0	π^0	ρ^0
							B_s^0	$K_{L/S}$	K^{*0}
12	$K^\pm$	$K^\pm$	π^0		V_{ud}	$K_{L/S}$	$K^\pm$	$\pi^\pm$	
		$K_{L/S}$	$\pi^\mp$				$K_{L/S}$	π^0	
					V_{ub}	B_s^0	$B^\pm$	$K^\pm$	$K^{*\pm}$
							B^0	$K_{L/S}$	K^{*0}
							B_s^0	$\eta^{(\prime)}$	ϕ
21	$D^\pm$	$D^\pm$	π^0	ρ^0	V_{cs}	$K_{L/S}$	$K^\pm$	$\pi^\pm$	
		D^0	$\pi^\mp$	$\rho^\mp$			$K_{L/S}$	π^0	
		$D_s^\pm$	$K_{L/S}$	K^{*0}	V_{cb}	B^0	$B^\pm$	$\pi^\pm$	$\rho^\pm$
							B^0	π^0	ρ^0
							B_s^0	$K_{L/S}$	K^{*0}

Table 3. All included N production modes of the form $M \to N + (e^\pm/\nu_e) + (M^{(*)\prime})$. We state the modes for the generational indices ij of the charged modes. For the neutral modes present in the leptoquark and RPV scenarios suppressed by the CKM matrix element V_{il}, the quark family indices are lj. We do not list the possible pion decay modes such as $\pi^\pm \to N + e^\pm$ for $ij = 11$, as pion-production in the very forward region is not well validated in `PYTHIA8`.

Lagrangians in eqs. (2.6) and (2.7) allow for invisible decays (only final-state neutrinos) and visible leptonic or semi-leptonic decays. For a relatively light N, the latter are dominated by decays into a single final-state meson plus a lepton. We consider the pseudoscalar mesons: π, K, η, η', D, D_s, η_c, and separately the vector mesons: ρ, K^*, ω, ϕ, D^*, D^*, J/ψ. For a heavier N, decays into multi-meson states become relevant and to estimate the total hadronic decay width we follow ref. [120] to calculate the decay rate into spectator quarks times appropriate loop corrections to account for the hadronization effects

$$\Gamma(N \to (e/\nu_e) + \text{hadrons}) = [1 + \Delta_{\text{QCD}}(m_N)] \times \Gamma_{\text{tree}}(N \to (e/\nu_e) + \bar{q}q)\,, \tag{5.1}$$

which includes both charged and neutral weak currents. The loop corrections are obtained from a comparison to hadronic τ decays and reproduced below [120, 125]

$$\Delta_{\text{QCD}}(m_N) = \frac{\alpha_s}{\pi} + 5.2\frac{\alpha_s^2}{\pi^2} + 26.4\frac{\alpha_s^3}{\pi^3}\,, \tag{5.2}$$

where $\alpha_s = \alpha_s(m_N)$. The hadronic decay width into multi-meson final states becomes relevant for N masses above 1 GeV roughly and we write as an approximation

$$\begin{aligned}\Gamma_N = \Gamma_{N\to\text{leptons}} &+ \Theta(1\,\text{GeV} - m_N)\,\Gamma_{N\to\text{single meson}} \\ &+ \Theta(m_N - 1\,\text{GeV})\,[1 + \Delta_{\text{QCD}}(m_N)]\,\Gamma_{N\to\bar{q}q}\,.\end{aligned} \tag{5.3}$$

Appendix A and refs. [122, 126] provide more detail on the explicit decay-rate calculations.

JHEP01(2024)108

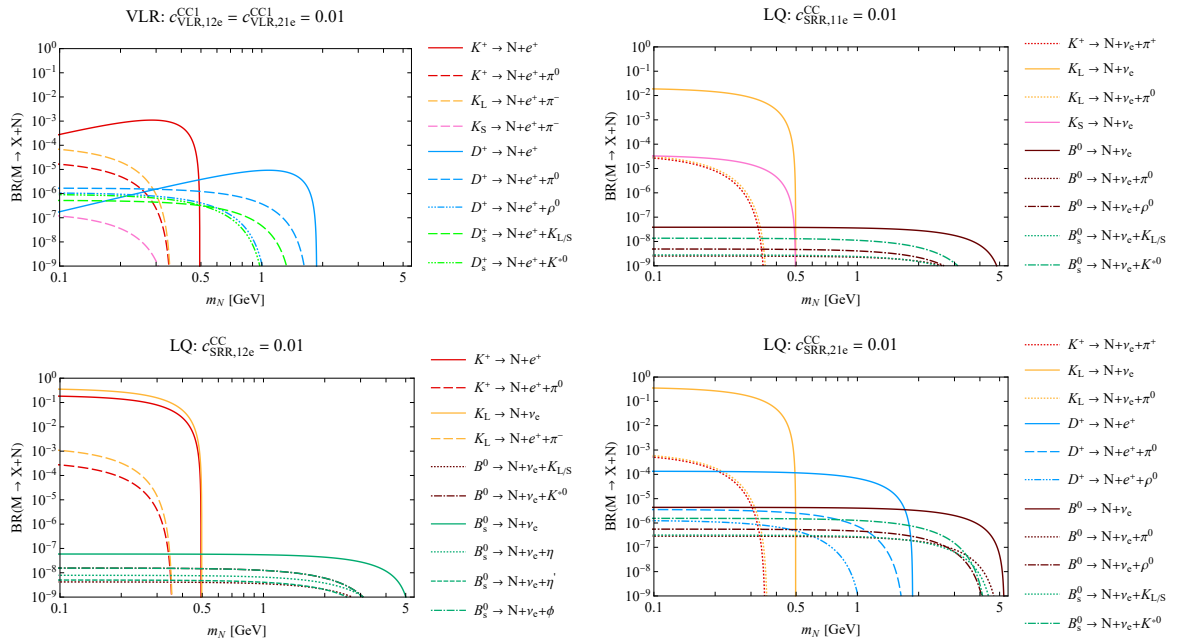

Figure 2. Branching ratios for the production of a GeV-scale N via the non-zero EFT-couplings of each scenario (specified in section 3) for various flavor benchmarks, with the related Wilson coefficients all set to 0.01. We neglect the contribution from a non-zero minimal mixing U_{e4}. The upper left depicts the meson decay modes of the left-right symmetric model-like scenario. The remaining three plots are for the leptoquark scenario, split into the flavor couplings ijk=111 (upper right), ijk=121 (lower left), and ijk=211 (lower right).

5.2 Effective operators

The νSMEFT operators contribute to a greater number of decay processes of an LLNF. In the theoretical scenarios under consideration, the most important additional decay modes involve a single final-state meson and a lepton.[5]

We list the allowed decays modes for each scenario and flavor benchmark in table 4, assuming the N is massive enough in each case. The proper decay length for each scenario and each flavor benchmark with a charged-current Wilson coefficient $c = 0.01$ and no minimal mixing, $U_{e4} = 0$, is plotted in figure 3. The remaining Wilson coefficients are then set according to eqs. (3.5)–(3.7). For the left-right symmetric model, the resulting decay lengths agree with those computed in ref. [45]. However for the leptoquark scenario, the decay lengths differ, as the neutral decay modes via the EFT couplings were not taken into account in that work. Because of the larger number of the available final states, the total decay rate of N increases and hence the decay length decreases accordingly. The numerical difference depends on the available modes based on the LLNF mass m_N. The explicit expressions for decays with two-body final states are provided in appendix A.

We stress that without minimal mixing U_{e4}, the decay lengths for the leptoquark and RPV scenario are identical for $m_N < 1\,\text{GeV}$. For masses larger than 1 GeV, the decay lengths

[5] Multi-meson final states can become important but are hard to control theoretically for scalar and tensor operators and therefore not included. The estimates of ref. [45] indicate that such modes are subdominant for N with a mass below 2 GeV and thus safe to neglect for DUNE.

JHEP01(2024)108

	Leptoquark / RPV			Left-Right
ij	$M^{\pm}$	M^0	$[V_{il}]$	$M^{\pm}$
11	$\pi^{\pm}$, $\rho^{\pm}$	π^0, ρ^0, η, η', ω	$[V_{ud}]$	$\pi^{\pm}$, $\rho^{\pm}$
		$K_{L/S}$, K^{*0}	$[V_{us}]$	
		B^0, B^{*0}	$[V_{ub}]$	
12	$K^{\pm}$, $K^{*\pm}$	$K_{L/S}$, K^{*0}	$[V_{ud}]$	$K^{\pm}$, $K^{*\pm}$
		η, η', ϕ	$[V_{us}]$	
		B_s^0, B_s^{*0}	$[V_{ub}]$	
21	$D^{\pm}$, $D^{*\pm}$	π^0, ρ^0, η, η', ω	$[V_{cd}]$	$D^{\pm}$, $D^{*\pm}$
		$K_{L/S}$, K^{*0}	$[V_{cs}]$	
		B^0, B^{*0}	$[V_{cb}]$	

Table 4. Possible decay modes for an LLNF N for each EFT scenario. We sort the modes by the generation indices ij of the charged quark current. Possible neutral quark currents have the indices lj and are suppressed by the stated CKM matrix element V_{il}. We fix the lepton index to $k = e$, so that the decays have the form $N \to M^{\pm} + e^{\mp}$ or $N \to M^0 + \nu_e$.

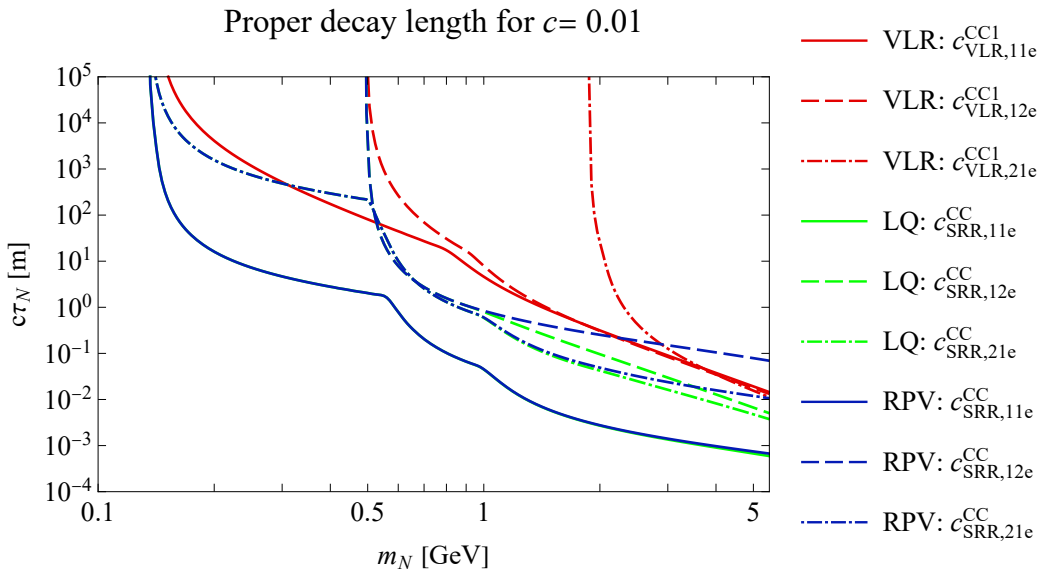

Figure 3. Proper decay length of N for all theoretical scenarios and different flavor couplings. We set the EFT couplings to $c = 0.01$ and turn off the minimal mixing ($U_{e4} = 0$).

for flavor coupling $ijk = 11e$ remain the same between the two scenarios, while for $ijk = 12e$ and $ijk = 21e$, the decay lengths start to differ as the contributions from the tensor couplings in these scenarios become more important.

6 The DUNE experiment

In this section, we briefly introduce the DUNE experimental setup. The experiment is comprised of a beamline facility at Fermilab in Illinois, USA, and an underground cryogenic detector

JHEP01(2024)108

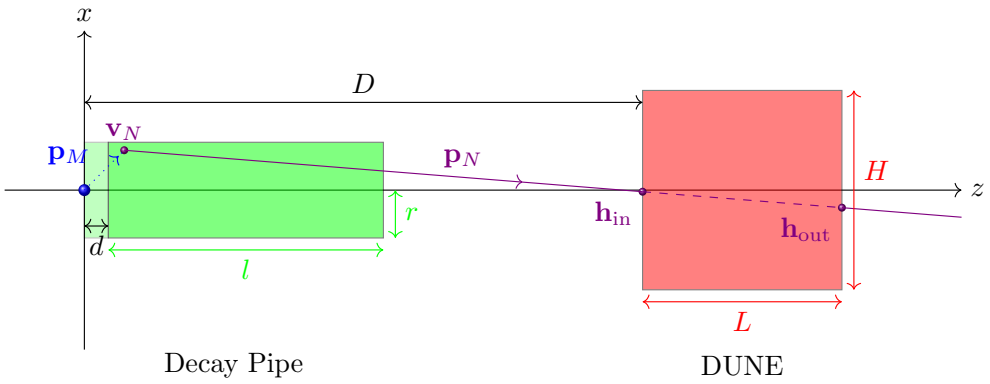

Figure 4. Schematic drawing of the DUNE near detector (red) and the decay pipe (green). An example event of a LLNF produced at a displaced vertex is included. A meson (dashed blue) traveling in direction $\vec{p}_M$ can decay at a displaced vertex $\vec{v}_N$ into an LLNF N (purple). The LLNF traveling in direction $\vec{p}_N$ can then be observed in the near neutrino detector. The geometric dimensions are given in table 5.

infrastructure at the Sanford Underground Research Facility (SURF) in South Dakota. The objective of the beamline facility is to provide a neutrino beam ideal for studying neutrino oscillation physics [6, 127–129]. To that end, a proton beam (60–120 GeV) is extracted from the Fermilab Main Injector. The beam collides with a graphite target generating a secondary beam of charged particles. For a beam-energy of 120 GeV the design allows for 1.1×10^{21} protons on target per year. The charged particles subsequently are sign-selected and focused with horns.[6] A 194 m long and 4 m wide decay pipe displaced 27 m downstream from the target provides space for the secondary beam to decay into neutrinos, or other LLNFs. Additionally, the beamline facility includes a conventional setup for a near-detector system (NDS) 574 m downstream from the target. The NDS consists of a beamline measurement system, a data acquisition system, and a fine-grained tracker (FGT) near neutrino detector (NND) with a tracking volume of 78.4 m^3. Important parameters such as geometrical sizes and reference beam parameters are listed in table 5. A schematic drawing of the beamline facility is shown in figure 4. For our numerical simulation, we fix the proton beam energy to be 120 GeV, and consider ten years' operation time corresponding to 1.1×10^{22} protons on target.

The focused neutrino beam travels approximately 1300 km towards the SURF. Because of the large distance between the target and the DUNE far detector, the latter is not suited for our topic of interest. We will instead focus on the DUNE near detector as a possibility to detect long-lived N's.

6.1 Monte-Carlo simulation

Considering the scenarios described in section 3, we are interested in the secondary beam of charged particles. The mesons produced in the proton-proton collisions may decay into LLNFs, N's. We perform Monte-Carlo (MC) simulations in order to evaluate the search

[6] In this work, to simplify the simulation, we do not consider the effect of the magnetic horns. The focusing effect would improve the number of mesons and hence the number of N's that could be detected by DUNE, so that our results are conservative.

JHEP01(2024)108

Reference beam parameters		geometrical variables	
proton beam energy	120 GeV	decay pipe length l	194 m
cycle time	1.2 s	decay pipe radius r	2 m
protons per cycle	7.5×10^{13}	distance: target - decay pipe d	27 m
spill duration	1.0×10^{-5} s	near detector length L	6.4 m
protons on target per year	1.1×10^{21}	near detector width H	3.5 m
		distance: target - near detector D	574 m

Table 5. Reference beam parameters and geometrical details of the beamline facility at Fermilab [128, 129].

Quark q	s	c	b
χ_q	1/7	1×10^{-4}	1×10^{-10}

Table 6. Fraction of quarks generated in the proton-target collisions at DUNE [130, 131].

sensitivity of the DUNE near detector to an N produced from a meson and subsequently decaying at a displaced vertex into a lighter meson.

First, we determine the number of N's produced in meson decays over the runtime of the DUNE experiment, which can be calculated in νSMEFT via the number N_M of any given meson M and its decay branching ratio into N:

$$N_{M,N}^{\text{prod}} = N_M \cdot \text{Br}(M \to N + X), \tag{6.1}$$

where X denotes any possible combination of leptons and lighter mesons. The branching ratios have been calculated in ref. [45] and in section 4. For the numbers of mesons produced at the experiment, we follow ref. [17], where the numbers of secondary hadrons are calculated by

$$N_M = N_{\text{POT}} \cdot M_{pp} \cdot \chi_q \cdot f_{q \to M}. \tag{6.2}$$

Here, N_{POT} is the number of protons on target over the runtime of the experiment. M_{pp} is the multiplicity of the proton-target reaction and indicates on average how many mesons M are produced in each primary proton-proton collision. χ_q is the fraction of quarks q generated at the primary vertex at a given beam energy with

$$\chi_q \equiv \frac{\sigma_{pp \to q}}{\sigma_{pp_{\text{total}}}}, \tag{6.3}$$

where $\sigma_{pp \to q}$ and $\sigma_{pp_{\text{total}}}$ denote the q-generation and inelastic scattering cross section, respectively. $f_{q \to M}$ is the fragmentation factor of the quark q into a meson M. The implemented values for χ_q and $f_{q \to M}$ are listed in tables 6 and 7, respectively.

For every meson except kaons, the multiplicity factor is already included in χ_q, so we set $M_{pp} = 1$ in these cases. For kaons and a beam energy of 120 GeV, we take $M_{pp} = 11$ [123]. The resulting meson numbers for a runtime of ten years are given in table 8.

JHEP01(2024)108

Quark q	s			c			b		
Meson M	K^-	K_L	K_S	D^+	D^0	D_s	B^+	B^0	B_s^0
$f_{q\to M}$	1/3	1/3	1/3	0.207	0.632	0.088	0.405	0.405	0.101

Table 7. Different quark fragmentation factors for kaons [123, 130], charm mesons [132], and bottom mesons [133].

Meson M	K^-	K_L	K_S
Number of Mesons	5.76×10^{21}	5.76×10^{21}	5.76×10^{21}
Meson M	D^+	D^0	D_s
Number of Mesons	2.28×10^{17}	6.95×10^{17}	9.68×10^{16}
Meson M	B^+	B^0	B_s^0
Number of Mesons	4.46×10^{11}	4.46×10^{11}	1.11×10^{11}

Table 8. Total numbers of mesons produced at DUNE over a runtime of ten years with 1.1×10^{22} POT, over a 4π solid angle coverage.

In order for the LLNF N to be observable, we require a 'visible' final state. 'Invisible' decay modes are those for which we expect DUNE not to be able to reconstruct the decay vertex. For the case of an N as a sterile neutrino in the minimal scenario, it mixes with electron neutrinos and the 'invisible' modes are $N \to \nu_e + \nu_i + \bar{\nu}_i$ with $i \in \{e, \mu, \tau\}$. Every other mode is considered as 'visible'. Additionally, the LLNF must decay inside the near detector. For an individual N produced by meson M, the probability for it to decay inside the fiducial volume can be calculated with the exponential decay law:

$$P_{M,i}[N \text{ in f.v.}] = \exp\left[-\frac{L_{T,i}}{\lambda_i}\right] \cdot \left(1 - \exp\left[-\frac{L_{I,i}}{\lambda_i}\right]\right), \tag{6.4}$$

where "f.v." stands for "fiducial volume", $L_{T,i}$ is the length that N travels to reach the detector, $L_{I,i}$ is the length it would take for the N to travel through the detector if it did not decay inside the fiducial volume, and λ_i is the boosted decay length of the i-th N simulated. The decay length is determined with the speed β_i, the boost factor γ_i, the speed of light c, as well as the LLNF proper lifetime τ_N, with $\lambda_i = \beta_i \gamma_i c \tau_N$. We employ MC techniques and simulate $N_{\text{MC}} = 10^6$ proton-on-target events with the event generator PYTHIA8 [134, 135] in order to obtain the average decay probability inside the detector for the N's produced from the meson M:

$$\langle P_M[N \text{ in f.v.}] \rangle = \frac{1}{N_{\text{MC}}} \sum_i^{N_{\text{MC}}} P_{M,i}[N \text{ in f.v.}]. \tag{6.5}$$

The number of observable N in the fiducial volume is then estimated with

$$N_N^{\text{obs}} = \text{Br}(N \to \text{visible}) \cdot \sum_M N_{M,N}^{\text{prod}} \cdot \langle P_M[N \text{ in f.v.}] \rangle \ , \tag{6.6}$$

where $\text{Br}(N \to \text{visible})$ denotes the visible decay branching ratio of N. We note, that we assume 100% detection efficiencies when calculating N_N^{obs}.

JHEP01(2024)108

6.2 Three-dimensional detector approximation

To calculate the individual decay probability within the detector of an LLNF, N_i, produced by a meson M, we require the lengths $L_{T,i}$ and $L_{I,i}$, which can be determined with the help of three spacial vertices: the production vertex of the N_i, $\vec{v}_{N,i}$,[7] the vertex $\vec{h}_{\text{in}}$ where the trajectory of N_i enters the fiducial volume of the detector, and the vertex $\vec{h}_{\text{out}}$ where the trajectory of N_i would exit the fiducial volume if N_i were not to decay inside the detector volume. For every generated particle P of the i-th event `PYTHIA8` provides a production vertex $\vec{v}_{P,i}$ and the orientation in terms of the momentum $\vec{p}_{P,i}$ of every generated particle P of the i-th event. We use the position $\vec{v}_{N,i}$ and $\vec{p}_{N,i}$, to describe the trajectory of any neutral particle N_i (unaffected by any electromagnetic field) with a (real scalar) parameter $s \geq 0$ as (see figure 4)

$$\vec{T}(s) = \vec{v}_{N,i} + s\,\vec{p}_{N,i}\,. \tag{6.7}$$

`DUNE` can be approximated as a cuboid. We define the fiducial volume of the `DUNE` near detector as enclosed by six areas defined via corner vertices $\vec{c}_j$ ($j = 1, \ldots, 8$). For every area, we take three of the four corners of that area ($\vec{c}_j$, $\vec{c}_{j'}$, and $\vec{c}_{j''}$) and calculate two directional vectors

$$\vec{o}_1 = \vec{c}_{j'} - \vec{c}_j\,, \qquad \vec{o}_2 = \vec{c}_{j''} - \vec{c}_j\,, \tag{6.8}$$

where $\vec{o}_1 \nparallel \vec{o}_2$. The plane in which the area lies can be described with two (real scalar) parameters t and u as

$$\vec{P}(t,u) = \vec{c}_j + t\,\vec{o}_1 + u\,\vec{o}_2. \tag{6.9}$$

Solving $\vec{T}(s) = \vec{P}(t,u)$ for s, t and u, we can determine the point $\vec{h}_{pl}$ where the plane $\vec{P}$ is hit. To determine if $\vec{h}_{pl}$ lies within the area of a bounding side of the fiducial volume or if the area is missed by the trajectory $\vec{T}(s)$, we perform the following steps of calculation (see figure 5):[8]

1. We determine the center $\vec{a}_c$ of the area as an average of all four corners $\vec{c}_j$, and the edge line equations $\vec{E}_j(a) = \vec{c}_j + a \cdot (\vec{c}_{j+1} - \vec{c}_j)$.

2. An imagined line between $\vec{a}_c$ and $\vec{h}_{pl}$ crosses every $\vec{E}_j(a)$. If $a \in (0,1)$ for the cross points $\vec{e}_{j,L}$, this cross point truly hits the edge of the area. Such a calculation results in two $\vec{e}_{j,L}$.

3. To find the $\vec{e}_{j,L}$ closer to $\vec{h}_{pl}$, we calculate the distance between center and both edge cross points $d_{E,j} = |\vec{e}_{j,L} - \vec{a}_c|$, as well as the distance between the hit point and edge cross point $d_{eh,j} = |\vec{e}_{j,L} - \vec{h}_{pl}|$. The $\vec{e}_{j,L}$, for which the sum of both distances is smaller, is the cross point closer to $\vec{h}_{pl}$.

4. Lastly, if $d_h = |\vec{h}_{pl} - \vec{a}_c| < d_{E,j}$, the hit point $\vec{h}_{pl}$ lies within the area. In other words, $\vec{T}(s)$ hits the fiducial volume in that area.

[7] 3-vectors are written in boldface. For LLNFs produced from kaons, because of the kaons' long lifetime, the production vertex is in most cases not the primary vertex. On the other hand, for charm and bottom meson decays, the production vertex can be approximated as coinciding with the primary vertex.

[8] In principle, for a cuboid it would be sufficient to check if $t, u \in (0,1)$, for $\vec{T}(s)$ to hit the fiducial volume. Our procedure can be extended to other geometric shapes and also approximate cylindrical detectors such as `ANUBIS` (see refs. [45, 97]).

JHEP01(2024)108

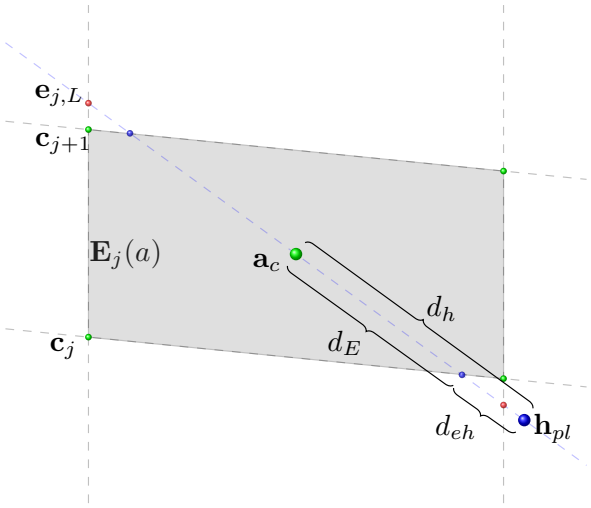

Figure 5. Sketch for determining, whether a particle trajectory hits a bounding side of the fiducial volume. The plane $\vec{P}$ is hit at $\vec{h}_{pl}$. Together with the center of the designated area $\vec{a}_c$ and the corner points $\vec{c}_j$, we can determine the intersection $\vec{e}_{j,L}$ (small red and blue dots) between the edges $\vec{E}_j(a)$ and a line through $\vec{a}_c$ and $\vec{h}_{pl}$. Subsequently, for the $\vec{e}_{j,L}$ closest to $\vec{h}_{pl}$ we can determine the distances $d_{E,j}$, $d_{eh,j}$, and d_h between the three vertices $\vec{a}_c$, $\vec{e}_{j,L}$, and $\vec{h}_{pl}$. If $d_h \leq d_{E,j}$ the designated area is hit.

These steps are repeated for every area until either all areas are checked, or two areas are found to be hit at $\vec{h}_{1/2}$, where $\vec{h}_1$ is the vertex closer to $\vec{p}_{N,i}$ and $\vec{h}_2$ is the vertex further. The required distances are then calculated as $L_{I,i} = |\vec{h}_2 - \vec{h}_1|$ and $L_{T,i} = |\vec{h}_1 - \vec{v}_{N,i}|$.

6.3 Kaons at the LHC

We are interested in comparing the sensitivity reach of DUNE to that of other experiments, especially (proposed) LHC far detectors such as FASER [136–138] and MATHUSLA [9, 139, 140]. For D- and B-mesons and only involving charged-current processes, these numerical results have already been obtained in ref. [45]. Implementing the geometry of these detectors in the simulation procedure explained in sections 6.1 and 6.2, we can extend the numerical results by including neutral couplings and production through kaon decays. To evaluate the sensitivity for such decays we need the total production cross sections of kaons at the LHC. We perform an estimate with the MC simulation tool EPOS-LHC [141], which is available in the CRMC simulation package [142], and obtain the following total kaon numbers at the LHC over the full 4π solid angle, for a center-of-mass energy 14 TeV, and an integrated luminosity of 3 ab^{-1}:

$$K_L = 1.30 \times 10^{18}, \qquad K_S = 1.31 \times 10^{18}, \qquad K^{\pm} = 2.38 \times 10^{18}. \tag{6.10}$$

We should treat the decay of kaons at the LHC with care. Heavier mesons, such as D- and B-mesons decay promptly and we can legitimately approximate the N as being produced at the interaction point (IP). Kaons, especially K_L and $K^{\pm}$, however, can travel a macroscopic distance before decaying. The algorithm specified in section 6.2 can account for the displaced N-production vertex. However, contrary to DUNE, the LHC does not include a decay pipe in which the long-lived mesons could decay. Depending on the experiment

JHEP01(2024)108

we investigate, the kaons could either enter a calorimeter or be absorbed by, for example, the surrounding rock wall. We do not simulate these possibilities. Instead, we restrict the allowed meson decay vertices $\vec{v}_{P,i}$ to be within a specific 'allowed decay region'. Such decay regions can be divided into different types:

- The first type of the decay regions is based on the hadron calorimetry (HCAL) of `CMS` [143] or `ATLAS` [144, 145]. `ANUBIS` [146] is supposed to be installed in a service shaft above `ATLAS`. A kaon that travels in the direction of `ANUBIS` necessarily enters the HCAL of `ATLAS`. We choose not to account for the effects of the HCAL on the kaons and therefore only consider kaons that decay before reaching the HCAL in our Monte-Carlo simulation. The inner radius of the barrel calorimeter HCAL at `ATLAS` is 2.28 m [144]. The end-cap calorimeter is placed ± 4.277 m from the IP in the direction of the beam axis. Hence, the allowed decay region for `ANUBIS` is restricted to a cylinder around the beam axis with the stated dimensions. Similarly, `MATHUSLA` would be located on the surface above the `CMS` experiment, which involves an HCAL. Here, the inner radius of the barrel calorimeter HCAL is 1.77 m, whereas the end-cap calorimeter is placed approximately ± 3 m from the IP. Similar to `ANUBIS`, the allowed decay region for kaons at `MATHUSLA` is a cylinder with the specified dimensions.

- Next, we discuss LLP detectors in the far forward region, namely, `FASER`, `FASER2`, and `FACET` [147]. These detectors are positioned downstream of the `ATLAS` or `CMS` IP. The beamlines close to the `ATLAS` and `CMS` IP's are almost identical [148]. Important for our purposes are the so-called 'Target Absorber Secondaries' (TAS) and 'Target Absorber Neutral' (TAN). These are absorbers for charged and neutral secondary particles in order to protect magnets and other machine elements of the beamline. Additionally, they can be used to reduce the background at LLP detectors [149]. Applied to our studies, the TAS and TAN limit the allowed decay region of charged and neutral kaons, respectively. The TAS is placed approximately 19 m after the IP, and the TAN's position is 141 m downstream from the IP. As `FACET` would be located closer to the IP than the respective TAN, namely, at 101 m, we only consider kaons which decay within 101 m, instead of the TAN's position.

- For `CODEX-b` [150], a specific lead shield is installed between the IP and the detector, covering the complete fiducial volume. The distance between the IP and the lead shield is approximately 5 m. Kaons are required to decay before reaching the shield in our simulation.

- The fourth decay region is relevant for `MAPP1` and `MAPP2` [151, 152]. Because of the location and shape of these detectors, we use the natural rock between the beam cavern and the detector cavern as the absorber for charged and neutral particles. Hence, kaons should decay inside the beam cavern, which is approximately 3.8 m wide.

7 Numerical results

We now present the results of the numerical simulation for the theoretical scenarios discussed in section 3. We begin with the minimal scenario where we only consider the active-sterile

JHEP01(2024)108

neutrino mixing and then subsequently discuss various scenarios where the long-lived neutral fermions have additional interactions. For each scenario we compare the reach of DUNE to that of other (proposed) experiments.

7.1 Minimal scenario

In the minimal scenario, N denotes specifically the sterile neutrino. The production and decay of light sterile neutrinos are both governed by the minimal mixing between sterile and active neutrinos. We do not employ the canonical see-saw relation $|U_{e4}|^2 = m_{\nu_e}/m_N$ and instead treat U_{e4} as a free parameter, together with the mass of the LLNF, m_N. We present the results of the numerical simulation (see section 6 for detail) in the $|U_{e4}|^2$ vs. m_N plane in figure 6. The DUNE sensitivity reach is compared to a range of other (proposed) experiments. The results are displayed as three-event isocurves, which correspond to the 95% confidence level (C.L.) sensitivity reach, assuming zero background events (see ref. [24] for a more nuanced discussion regarding backgrounds). The figure also shows a brown band representing the target region for the type-I seesaw relation $|U_{e4}|^2 = m_\nu/m_N$, where $0.05\,\text{eV} < m_\nu < 0.12\,\text{eV}$ [153, 154]. Further, we include current limits on $|U_{e4}|^2$ [155] from various experiments, shown in the light gray area, combining the results from PIENU [156], KENU [157], NA62 [158], T2K [159], BEBC [160], and DELPHI [161]. We also display the lower bounds expected from Big Bang Nucleosynthesis [162], as a dashed dark grey curve; note that these limits depend on the cosmological model considered. One shortcoming of our simulations is that we do not include sterile neutrino production through pion decays. Therefore, our results underestimate the sensitivity reach for $m_N < m_\pi \simeq 140\,\text{MeV}$, and this region is marked in red.

The DUNE isocurve can be split into two segments, where different production modes govern the sensitivity reach. For $m_\pi < m_N < m_K$ it is dominated by sterile neutrinos produced in kaon decays, because the number of kaons produced at DUNE is roughly four orders of magnitude larger than that of charmed mesons (see table 8). For $m_K < m_N < m_{D_s}$, kaon decays into the LLNF are no longer kinematically allowed, hence the kink in the sensitivity curves. The production is then dominated by the decays of charmed mesons. The peak sensitivity here is a bit above 1 GeV, because there the branching ratio for $D^\pm$ and D_s into a $N + e$ final state is the largest (cf. figure 1). For sterile neutrinos with masses above m_{D_s}, only N production modes via bottom meson decays are allowed. However, the number of bottom mesons produced at DUNE is so small, that the three-event isocurve does not extend into the region of this plot. Our sensitivity estimates are, apart from the region below the pion mass, in good agreement with, for example, refs. [17, 20] confirming the validity of our simulation.

As shown in figure 6, compared to the (proposed) detector concepts at the LHC, DUNE is expected to perform better than many of them for the minimal scenario. In the 'charmed'-region of the isocurve, only ANUBIS and MATHUSLA extend beyond the parameter region covered by DUNE, by less than one order of magnitude in $|U_{e4}|^2$. In the 'kaon'-region, DUNE is expected to probe $|U_{e4}|^2$ values smaller than what MATHUSLA and ANUBIS can do by almost one order of magnitude. It can even cover the see-saw band range for m_N between 0.2 GeV and 0.5 GeV. On the other hand, because of the much larger center-of-mass energy, the isocurve of every LHC detector concept except FASER extends beyond DUNE for masses above m_{D_s}, complementing DUNE's strong sensitivities at lower mass regions.

JHEP01(2024)108

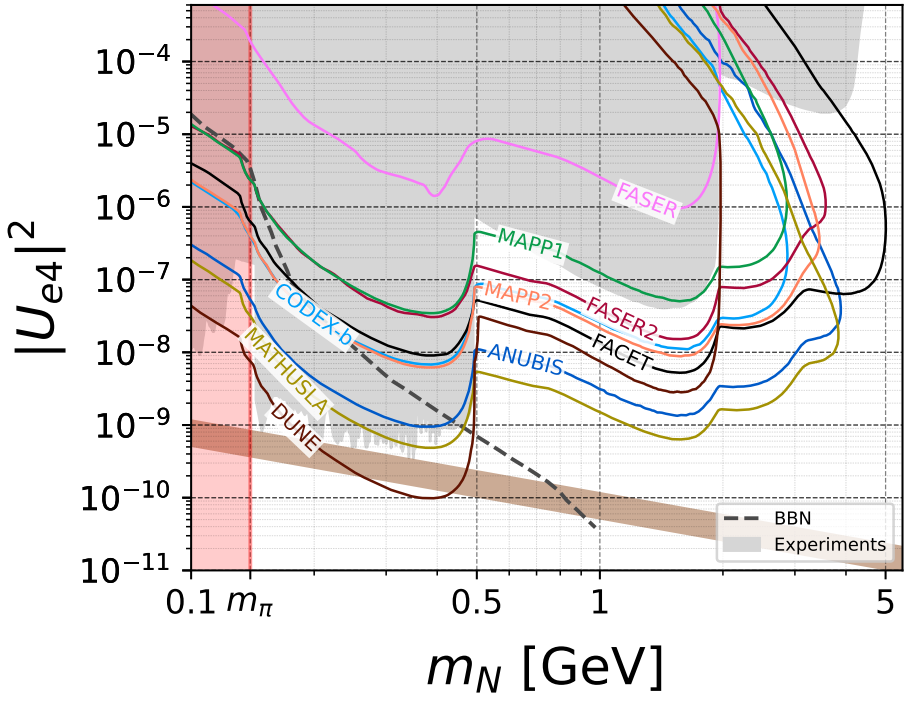

Figure 6. Sensitivity isocurves of DUNE and (proposed) LHC far detectors for the minimal scenario, shown in the plane $|U_{e4}|^4$ vs. m_N. The brown band indicates a target region for the type-I seesaw relation $|U_{e4}|^2 = m_\nu/m_N$, for $0.05\,\text{eV} < m_\nu < 0.12\,\text{eV}$. The light gray area and dark gray curve represent current limits on U_{e4} from experiments and the lower bounds from Big Bang Nucleosynthesis [162], respectively. The red area on the left corresponds to m_N below the pion threshold, where, in principle, contributions from pion decays could enhance the sensitivities but are not considered in the present work.

7.2 Flavor benchmarks

In each theoretical scenario we select different flavor benchmarks as discussed in section 4.2 and section 5.2. We select one EFT operator $(c_P)_{ij}$ *mainly* responsible for the production and another operator $(c_D)_{i'j'}$ for the decay of the N, where $i^{(\prime)}$ and $j^{(\prime)}$ are generation indices of the up- and down-type quarks of the charged νLEFT current, respectively. In the left-right symmetric model scenario, the operator is given by c_{VLR}^{CC1} with various flavor indices. For the leptoquark and the RPV-SUSY scenarios, we choose a specific flavor of the charged scalar operator c_{SRR}^{CC}, and further include the three related operators as described in eq. (3.5) and eq. (3.7). Contributions from active-sterile neutrino mixing U_{e4} are taken into consideration for the leptoquark and left-right symmetric model-like scenario using the canonical see-saw relation

$$U_{e4} = \sqrt{\frac{m_{\nu_e}}{m_N}}, \tag{7.1}$$

with a representative active neutrino mass $m_{\nu_e} = 0.05\,\text{eV}$ for both DUNE and the LHC far detectors. For DUNE, we additionally perform simulations where we turn off minimal mixing. We observe essentially no difference between the leptoquark scenario without minimal mixing

JHEP01(2024)108

	Leptoquark / RPV	Left-Right
$(c_P)_{ij}$ $(c_D)_{i'j'}$	$c^{CC}_{\mathrm{SRR},12}$ $c^{CC}_{\mathrm{SRR},11}$	$c^{CC1}_{\mathrm{VLR},12}$ $c^{CC1}_{\mathrm{VLR},11}$
N Production Modes via $\mathbf{M}$		
$\mathbf{M} \to N + e^{\pm}(+X)$	$K^{\pm}$, $K_{L/S}$	$K^{\pm}$, $K_{L/S}$
$\mathbf{M} \to N + \nu_e(+X)$ via CKM $[V_{il}]$	$K^{\pm}$, $K_{L/S}$ $[V_{us}, V_{ud}]$ $B^{\pm}$, B^0, B^0_s $[V_{ub}]$	
N Decay Modes into $\mathbf{M}'$		
$N \to \mathbf{M}' + e^{\pm}$	$\pi^{\mp}$, $\rho^{\mp}$, $K^{\mp}$, $K^{*\mp}$	$\pi^{\mp}$, $\rho^{\mp}$, $K^{\mp}$, $K^{*\mp}$
$N \to \mathbf{M}' + \nu_e$ via CKM $[V_{il}]$	π^0, ρ^0, ω $[V_{ud}]$ η, η' $[V_{us}, V_{ud}]$ $K_{L/S}$, K^{*0}, ϕ $[V_{us}]$ B^0, B^{*0}, B^0_s, B^{*0}_s $[V_{ub}]$	

Table 9. Summary of flavor benchmark 1 for theoretical scenarios 2, 3 and 4 as described in section 4 and section 5. Listed are the non-zero couplings $(c)_{P/D}$ as well as the induced N production and decay modes. X represents any possible additional final-state particle in the meson decays. Modes induced by related neutral quark currents are suppressed by the corresponding CKM matrix element. We do not list the contributions from a non-zero U_{e4} (see section 4.1 and section 5.1 for details).

and the RPV-SUSY scenario for every benchmark. The different relations between the scalar and tensor couplings in such scenarios [eq. (3.5) and eq. (3.7)], both in signs and in coupling strength, do not significantly affect the estimated number of observed N events. This aligns with the discussions in section 4.2 and section 5.2. Both the production and decay modes for an LLNF in the leptoquark scenario without minimal mixing and the RPV-SUSY scenario are comparable (see also figure 3), so that differences in the numerical results are minor. Thus, we only show the leptoquark results.

Furthermore, we reinterpret existing limits on the active-sterile mixing U_{e4} from meson decays in terms of the benchmark scenarios [52]. For sterile neutrinos with a mass $m_\pi < m_N < m_D$, we use the U_{e4}-limits from `NA62` [158], `T2K` [159], and `BEBC` [160], where N is produced in the decay of kaons or D-mesons. We assume U_{e4} is fixed according to eq. (7.1), with $m_{\nu_e} = 0.05\,\mathrm{eV}$ in the reinterpretation. The limits on the EFT operators obtained in this procedure are included in the following.

7.2.1 Flavor benchmark 1

In the first flavor benchmark, we consider for the production $(c_P)_{12} \in \{c^{CC}_{\mathrm{SRR},12}\,; c^{CC1}_{\mathrm{VLR},12}\}$ and for the decay $(c_D)_{11} \in \{c^{CC}_{\mathrm{SRR},11}\,; c^{CC1}_{\mathrm{VLR},11}\}$, for each respective scenario. The resulting meson and N decay modes are summarized in table 9. Meson decay modes, as given in eqs. (4.2)–(4.3), are induced by kaons, while we include kaons and B-meson decays via eqs. (4.4)–(4.5), if neutral couplings are non-zero in the specific scenario. Contributions

JHEP01(2024)108

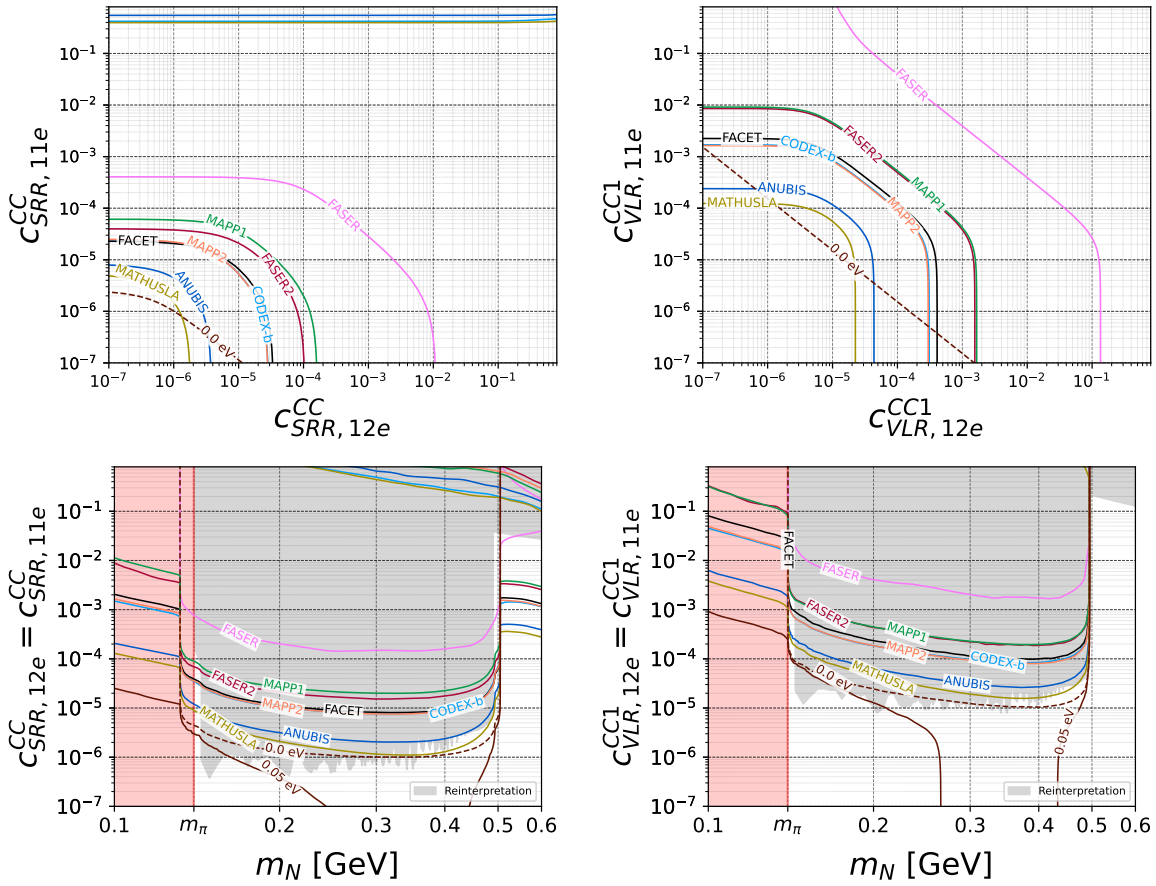

Figure 7. Sensitivity isocurves for flavor benchmark 1 as summarized in table 9. *Upper*: c_D vs. c_P for a fixed mass of $m_N = 0.3\,\text{GeV}$. *Lower*: $c_P = c_D$ vs. m_N. *Left*: the leptoquark and RPV scenarios. *Right*: the left-right symmetric model-like scenario. For all detectors, we show HNL sensitivity curves with the type-I seesaw relation for an active neutrino mass $m_\nu = 0.05\,\text{eV}$. Additionally, for DUNE, we display the results for $m_\nu = 0.0\,\text{eV}$, which also represent the sensitivity of the RPV-SUSY scenario, to a good approximation. We reinterpret existing limits on U_{e4} following ref. [52]. The light gray area represents the restricted parameter space obtained from the reinterpretation.

from a non-zero U_{e4} are not listed specifically, but included as described in section 4.1. We present results for the first benchmark in figure 7, where we show 3-signal-event isocurves as the sensitivity reach at 95% C.L..

The upper half of the figure contains two plots in the $(c_D)_{11}$ vs. $(c_P)_{12}$ plane, for a fixed mass $m_N = 0.3\,\text{GeV}$. The lower half contains two plots in the plane $(c_D)_{11} = (c_P)_{12}$ vs. m_N. In these plots, as discussed in section 7.2, we have followed ref. [52] and reinterpreted existing HNL searches in order to obtain recast bounds on the considered νLEFT scenario; these results are shown in light gray. The left side in each half shows results for the leptoquark (and RPV) scenarios, while the right side is for the left-right symmetric model-like scenario.

In the upper row, the DUNE isocurves for a neutrino mass $m_\nu = 0.05\,\text{eV}$ are missing. The reason for this is that in the minimal scenario, for such an active neutrino mass and $m_N = 300\,\text{MeV}$, the number of observed neutrino events is always greater than three independent of the EFT couplings. This also explains why the DUNE-isocurve here behave differently than the LHC-detector curves, as the latter do include minimal mixing.

JHEP01(2024)108

For this flavor benchmark, DUNE essentially outperforms all LHC detectors across the parameter space. This is clearly seen in the bottom panels, where the DUNE curves probe the smallest couplings. MATHUSLA and ANUBIS are not much weaker in sensitivity, though.[9] Because of neutral-current processes and the resulting B-meson decays into N, the LHC detectors isocurves extend beyond m_K to the right and complement DUNE's sensitivity reach. This can be observed in the lower-left plot of figure 7. We find for LLNF mass below the kaon threshold, essentially only DUNE and MATHUSLA can probe parameter space beyond the existing bounds.

Comparing the leptoquark scenario to the left-right symmetric model-like scenario, we find the sensitivity results of the left-right symmetric model-like scenario to be weaker than those of the leptoquark or RPV-SUSY scenario; the main reason is that the meson decay branching ratios for the LLNF production are enhanced in case of scalar-current interactions. This difference is even more pronounced for smaller neutrino masses, because of the chiral suppression of the vector operators in the left-right symmetric model-like scenario.

Additionally, in the lower plots of figure 7, the DUNE curve with $m_\nu = 0.0\,\text{eV}$ in the left-right symmetric model-like scenario (the right panel), shows a similar m_N-dependence to the LHC-detector sensitivity curves (with $m_\nu = 0.05\,\text{eV}$). However, in the leptoquark scenario, the $m_\nu = 0.0\,\text{eV}$ DUNE curve exhibits a slightly different m_N-dependence than the LHC-detector sensitivities with non-zero minimal mixing. This is explained by interference between N production modes arising from $(c_P)_{12}$ and U_{e4} which are included for the LHC detectors but not for the DUNE $m_\nu = 0.0\,\text{eV}$ line.[10] This interference is smaller in the left-right scenario and therefore the DUNE $m_\nu = 0.0\,\text{eV}$ line has the same m_N dependence as that of the LHC detectors in the bottom-right panel.

The DUNE RPV-SUSY results for this benchmark coincide with the $m_\nu = 0.0\,\text{eV}$ results shown in the lower-left plot, and have been worked out recently in ref. [72], where a quick and simple recast was performed; we find the results to be comparable to the results from the full simulations of this work.

Very roughly, DUNE will have a sensitivity range to νLEFT scalar couplings at the $C_{\text{SRR}}^{CC} \sim 10^{-6}$-level and to vector couplings at the $C_{\text{VLR}}^{CC1} \sim 10^{-5}$-level. This approximately corresponds to a BSM physics scales of $\Lambda \sim \sqrt{v^2/C_{\text{SRR}}^{CC}} = \mathcal{O}(250)\text{TeV}$ and $\Lambda \sim \sqrt{v^2/C_{\text{VLR}}^{CC1}} = \mathcal{O}(80)\text{TeV}$, respectively, for N masses around 0.3 GeV. These limits are stronger than many existing and proposed probes of νSMEFT couplings; see e.g. refs. [45, 114, 155], and, for this benchmark scenario, comparable to limits from NA62.

7.2.2 Flavor benchmark 2

We now consider production through $(c_P)_{21} \in \{c_{\text{SRR},21}^{CC}\,; c_{\text{VLR},21}^{CC1}\}$, while the decay coupling is unchanged $[(c_D)_{11}]$. The LLNFs are produced from charged-current D-meson decays, while production through kaon and B-meson decays can occur through neutral currents in the leptoquark and RPV scenarios. A summary is given in table 10.

[9] The sensitivity reaching down to zero coupling is here related solely to the minimal mixing contribution.

[10] We consider $(c_P)_{12} > 0$, so that the interference enhances the sensitivity for a non-zero U_{e4}. In principle, $(c_P)_{12} < 0$ or $U_{e4} < 0$ is allowed, such that the interference term could instead weaken the sensitivity reach for these detectors.

JHEP01(2024)108

	Leptoquark / RPV	Left-Right
$(c_P)_{ij}$ $(c_D)_{i'j'}$	$c^{CC}_{\mathrm{SRR},21}$ $c^{CC}_{\mathrm{SRR},11}$	$c^{CC1}_{\mathrm{VLR},21}$ $c^{CC1}_{\mathrm{VLR},11}$
N Production Modes via $\mathbf{M}$		
$\mathbf{M} \to N + e^{\pm}(+X)$	$D^{\pm}$, D^0, $D_s^{\pm}$	$D^{\pm}$, D^0, $D_s^{\pm}$
$\mathbf{M} \to N + \nu_e(+X)$ via CKM $[V_{il}]$	$K^{\pm}$, $K_{L/S}$ $[V_{us}, V_{cs}]$ $B^{\pm}$, B^0, B_s^0 $[V_{ub}, V_{cb}]$	
N Decay Modes into $\mathbf{M}'$		
$N \to \mathbf{M}' + e^{\pm}$	$\pi^{\mp}$, $\rho^{\mp}$, $D^{\mp}$, $D^{*\mp}$	$\pi^{\mp}$, $\rho^{\mp}$, $D^{\mp}$, $D^{*\mp}$
$N \to \mathbf{M}' + \nu_e$ via CKM $[V_{il}]$	π^0, ρ^0, η, η', ω $[V_{ud}, V_{cd}]$ $K_{L/S}$, K^{*0} $[V_{us}, V_{cs}]$ B^0, B^{*0}, B_s^0, B_s^{*0} $[V_{ub}, V_{cb}]$	

Table 10. Summary of flavor benchmark 2 for theoretical scenarios 2, 3, and 4 as described in section 4 and section 5.

Results for benchmark scenario 2 are given in figure 8 using the same panel formats as in figure 7. The upper plots spanned by $(c_D)_{11}$ and $(c_P)_{21}$ correspond to a fixed LLNF mass of 1 GeV. For this mass, we can include the DUNE sensitivity for a non-zero minimal mixing corresponding to the 0.05 eV line, which has a similar shape as the curves for the LHC detectors.

For a 1 GeV LLNF, the MATHUSLA and ANUBIS experiments outperform DUNE in sensitivity by roughly an order of magnitude in both production and decay EFT couplings. The reason is that the production rate of D-mesons at DUNE is only an order-of-magnitude greater than at the LHC experiments (whereas DUNE has a three-to-four order-of-magnitude gain for kaons). The larger angular coverage of MATHUSLA and ANUBIS in comparison to DUNE then results in the increased sensitivity for the LHC experiments. This is further reflected in the bottom panels where for N's heavier than kaons, the DUNE isocurves are above the MATHUSLA and ANUBIS lines (but still below many other experiments).

The production of LLNFs through kaon decays (even when setting $U_{e4} = 0$) still leads to DUNE being the most sensitive experiment for N's lighter than a kaon. The mass-dependence for the leptoquark-model (and RPV model) with $m_\nu = 0.0\,\mathrm{eV}$ is now very similar to the LHC-detectors where $U_{e4} \neq 0$ because interference effects play no significant role in this benchmark. The production through kaon decays from the EFT operators however does not work in the left-right scenario. As such, without minimal mixing, MATHUSLA and ANUBIS outperform DUNE in this scenario even for light LLNFs as shown in the bottom-right panel.

Finally, the recast bounds shown in the light gray area are much weaker than several of the experiments considered here. This is mainly caused by the fact that the EFT operators in this benchmark do not contribute to the two-body decay $K^{\pm} \to N + e^{\pm}$, and therefore the NA62 limits do not apply.

JHEP01(2024)108

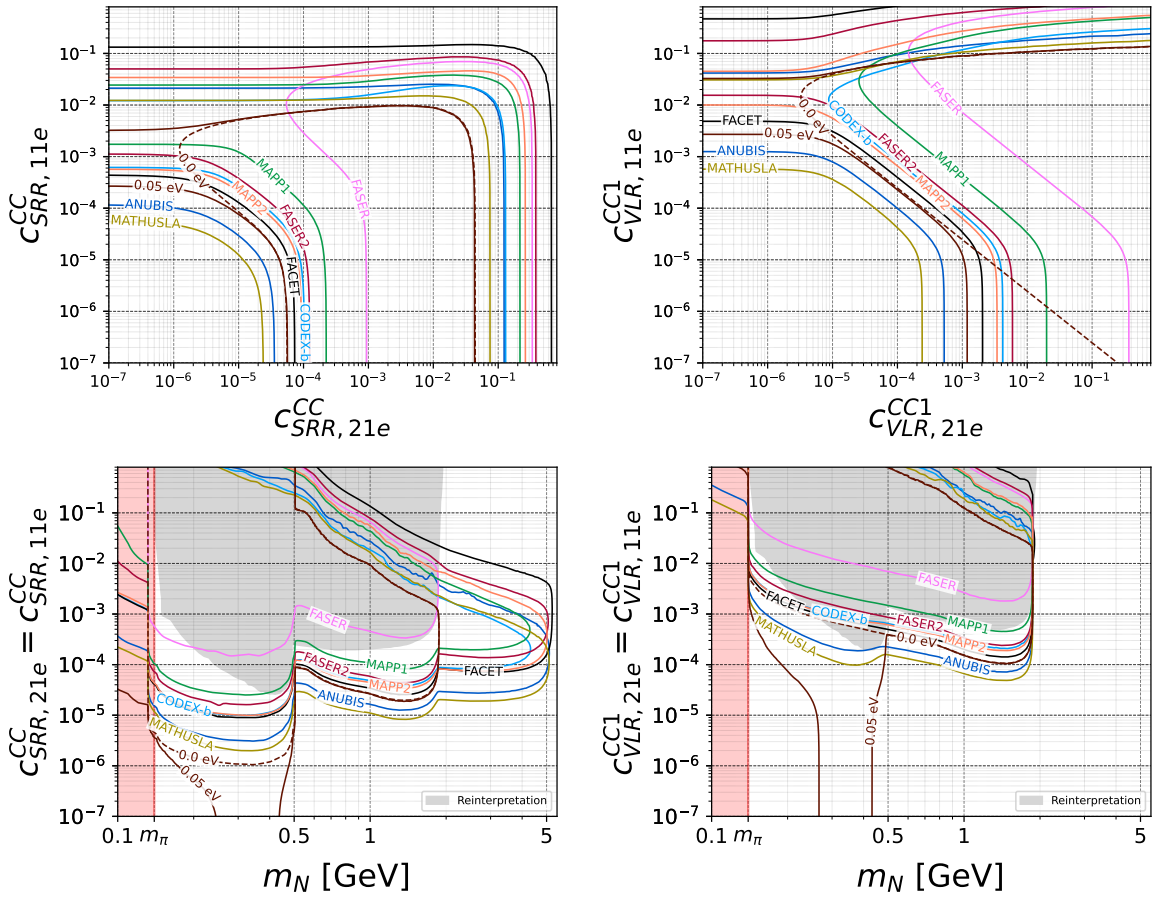

Figure 8. DUNE sensitivity isocurves for flavor benchmark 2. The three-event isocurves (at 95% C.L.) depend on the individual couplings strengths c_P and c_D, as well as the LLNF mass m_N. In the upper row, we fix $m_N = 1.0\,\text{GeV}$ and display the results as c_P vs. c_D. In the lower row, we restrict $c_P = c_D$ and show the isocurves in the c_P vs. m_N plane. On the left side, the leptoquark and RPV scenarios are depicted, while the left-right symmetric model-like scenario is shown on the right. We include together sensitivity isocurves for several previously investigated LHC detector proposals [45] that we expand on here. The light gray area represents excluded parameter space obtained by reinterpreting existing U_{e4} limits.

7.2.3 Flavor benchmark 3

In the final benchmark scenario, we consider production of the LLNFs through $(c_P)_{21}$ and decays through $(c_D)_{12}$, leading to production and decay modes summarized in table 11. The sensitivity isocurves are shown in figure 9. In the $(c_D)_{12}$ vs. $(c_P)_{21}$ plane, the structure of the sensitivity curves is very similar to that in figure 8, so in the interest of brevity, we do not show these plots here.

For the leptoquark and RPV scenarios, the results are similar compared to the previous benchmark except that the DUNE $m_\nu = 0.0\,\text{eV}$ curve now is somewhat above the MATHUSLA curve for light LLNFs (this was the other way around in the previous benchmark). For very small EFT couplings, the decay length is large and the probability, see eq. (6.4), for an LLNF to decay inside the detector is approximately

$$P_N = \exp\left[-L_T/\lambda_N\right] \cdot \left(1 - \exp\left[-L_I/\lambda_N\right]\right) \simeq L_I/\lambda_N \;\propto\; L_I \cdot \Gamma^N_{\text{tot}}\,, \tag{7.2}$$

JHEP01(2024)108

	Leptoquark / RPV	Left-Right
$(c_P)_{ij}$ $(c_D)_{i'j'}$	$c^{CC}_{\mathrm{SRR},21}$ $c^{CC}_{\mathrm{SRR},12}$	$c^{CC1}_{\mathrm{VLR},21}$ $c^{CC1}_{\mathrm{VLR},12}$
N Production Modes via $\mathbf{M}$		
$\mathbf{M} \to N + e^{\pm}(+X)$	$K^{\pm}$, $K_{L/S}$, $D^{\pm}$, D^0, $D_s^{\pm}$	$K^{\pm}$, $K_{L/S}$, $D^{\pm}$, D^0, $D_s^{\pm}$
$\mathbf{M} \to N + \nu_e(+X)$ via CKM $[V_{il}]$	$K^{\pm}$, $K_{L/S}$ $[V_{ud}, V_{cs}]$ $B^{\pm}$, B^0, B_s^0 $[V_{ub}, V_{cb}]$	
N Decay Modes into $\mathbf{M}'$		
$N \to \mathbf{M}' + e^{\pm}$	$K^{\mp}$, $K^{*\mp}$, $D^{\mp}$, $D^{*\mp}$	$K^{\mp}$, $K^{*\mp}$, $D^{\mp}$, $D^{*\mp}$
$N \to \mathbf{M}' + \nu_e$ via CKM $[V_{il}]$	π^0, ρ^0, ω $[V_{cd}]$ η, η' $[V_{us}, V_{cd}]$ ϕ $[V_{us}]$ $K_{L/S}$, K^{*0} $[V_{cs}]$ B^0, B^{*0} $[V_{cb}]$ B_s^0, B_s^{*0} $[V_{ub}]$	

Table 11. Summary of flavor benchmark 3 for theoretical scenarios 2, 3, and 4 as described in section 4 and section 5.

and thus proportional to the total decay rate. For light LLNFs and small EFT couplings, in this benchmark the minimal mixing actually dominates Γ^N_{tot}. This explains why the DUNE $m_\nu = 0.0\,\mathrm{eV}$ curve falls below the MATHUSLA curve where minimal mixing is included. This is more pronounced in the left-right scenario without minimal mixing where for $m_N < m_K$, the LLNF is stable and thus the $m_\nu = 0.0\,\mathrm{eV}$ curve does not reach this region at all.

For larger masses, however, the limits between flavor benchmarks 2 and 3 are very similar and reach 10^{-4} in the couplings, about an order of magnitude weaker than in benchmark 1, because of the lower production rates of the charmed mesons at DUNE. The recast bounds from existing HNL searches outperform most of the considered experiments for m_N below the kaon threshold, while for $m_K \leq m_N \leq m_{D_s}$, the proposed LHC detectors and DUNE will do a lot better than existing searches.

8 Conclusions

In recent years, perhaps driven by the non-observation of heavy beyond-the-Standard-Model (BSM) states at the LHC, more attention has shifted towards hypothetical light and feebly-interacting new particles. These elusive particles can play a role in solving outstanding problems of the Standard Model (SM) such as neutrino masses and/or dark matter. In this work, we have focused on long-lived neutral fermions (LLNFs), which are predicted in various BSM models. We show that LLNFs which are SM-singlets, can be described, in a

JHEP01(2024)108

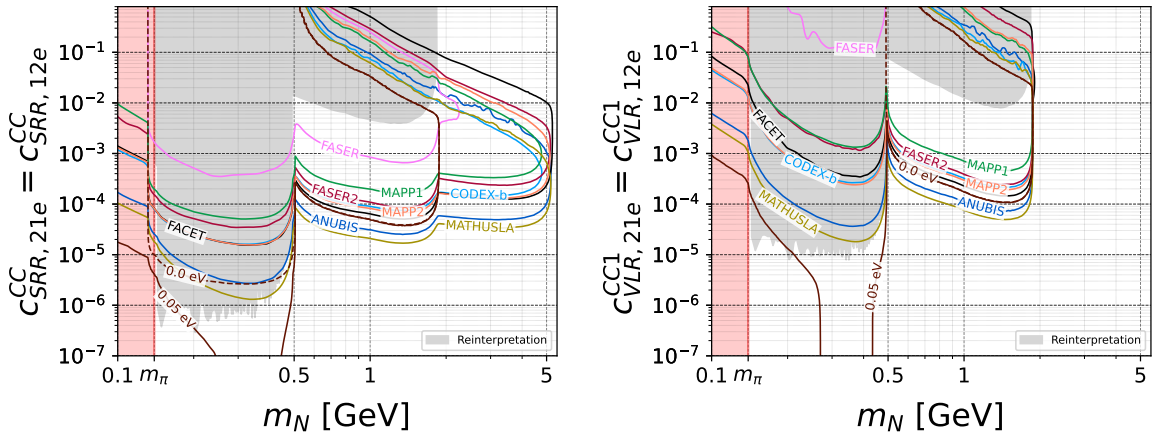

Figure 9. DUNE sensitivity isocurves for flavor benchmark 3. We do not present the isocurves for $(c_D)_{12}$ vs. $(c_P)_{21}$ as the sensitivity curves at $m_N = 1\,\text{GeV}$ are very similar to those shown in figure 8. On the left-side (right-side) we display the isocurves in the $(c_P)_{21} = (c_D)_{12}$ vs. m_N plane for the leptoquark/RPV-SUSY (left-right symmetric) model. The light gray area represents limits on the EFT operators reinterpreted from existing upper bounds on U_{e4}.

unified way, in terms of neutrino-extended Standard Model Effective Field Theory (νSMEFT) and its low-energy counterpart νLEFT. For illustration purpose, here, we have focused on two sample cases: heavy neutral leptons (HNLs) and the lightest neutralinos in the R-parity-violating supersymmetry (RPV-SUSY).

In minimal models, the HNLs interact solely through mixing with active neutrinos, but in other scenarios they can have very different interactions with SM fields, for example, through the exchange of BSM particles. Assuming the latter to be heavy, at low energies the HNL phenomenology can be described by the νSMEFT Lagrangian. In supersymmetric scenarios, the lightest neutralinos are necessarily bino-like and hence SM-singlets. They have to decay to avoid overclosing the Universe, which can be realized, e.g. in RPV-SUSY. Integrating out heavy supersymmetric fields, the interactions of the lightest neutralino can then also be described by the same νSMEFT framework. In this light, the name, neutrino-extended SMEFT, is a bit of a misnomer since it can be efficiently used to describe LLNFs that are not related to neutrino physics at all. We have derived matching relations between the UV-complete theory (RPV-SUSY) and the νSMEFT/νLEFT to illustrate this point.

The main purpose of this work has been to investigate the potential of the neutrino experiment DUNE to detect LLNF's, and compare the DUNE reach to other (proposed) experiments. At the DUNE experiment, large numbers of strange and charm mesons are produced that can potentially decay into LLNFs such as the HNLs or the lightest neutralinos. We have investigated four scenarios in detail: the first one is the usual minimal scenario of the HNLs, where we assume that the HNLs mix with the electron neutrinos only. This scenario has been studied multiple times in the literature before and we mainly use this as a benchmark to verify our calculations and simulation tools: indeed our estimated sensitivities are close to those reported in e.g. refs. [17, 20]. In the second and third scenarios we use the νSMEFT and νLEFT frameworks to investigate more general interactions. In particular we focus on scalar- and tensor-like charged current operators, that are, for example, induced in leptoquark models, and a left-right vector-like operator that is induced in left-right symmetric models.

JHEP01(2024)108

The fourth scenario is the above-mentioned light bino in RPV-SUSY. In each scenario we have investigated the role of different flavor assignments which is rather important for the comparison between DUNE and LHC experiments.

We have performed detailed Monte-Carlo simulations and computations to obtain the predicted signal-event rates of the rare decays of the LLNFs in different scenarios inside the DUNE near detector (DUNE-ND). Given the expected vanishing background, we have presented the sensitivity reach at 95% confidence level corresponding to three signal events. For LLNFs produced from kaons that are long-lived themselves, we have developed an algorithm that takes into account the decay position of the kaons instead of assuming that the LLNFs are produced at the interaction point. With this method, we have estimated the sensitivities of both the DUNE-ND and the proposed LHC far detectors to the HNLs for both minimal scenarios and more complicated extensions in a consistent way.

Our main conclusion is that DUNE will be extremely sensitive to LLNF's with masses below roughly 2 GeV (the D_s threshold). In particular, for masses below the kaon mass, DUNE's sensitivity reach even exceeds that of the largest proposed LHC experiment, MATHUSLA. This holds for the minimal scenario and the RPV-SUSY model, and typically also for general νSMEFT scenarios. However, in certain flavor benchmarks where the LLNF production through kaon decays is relatively suppressed, the LHC experiments MATHUSLA and ANUBIS are projected to do better because of the difference in relative production rate of heavier mesons compared to kaons at the LHC. This also explains why these experiments typically perform somewhat better than DUNE in the $0.5 - 2$ GeV LLNF mass range. However, the difference is not very large and the DUNE sensitivity reach is still excellent. Our study exemplified the usefulness of studying LLNFs which are SM-singlets in the theoretical framework of effective field theories, and motivates the search for long-lived fermions at the DUNE-ND.

Acknowledgments

We thank Martin Hirsch and Oliver Freyermuth for useful discussions. Financial support for H.K.D. by the DFG (CRC 110, "Symmetries and the Emergence of Structure in QCD") is gratefully acknowledged. JdV acknowledges support from the Dutch Research Council (NWO) in the form of a VIDI grant.

A Meson decay rate calculation

The dimension-6 operators of the effective Lagrangian (eq. (2.6) and eq. (2.7)) at tree-level allow for meson decays with two-body or three-body final states involving heavy neutral leptons. Through the same operators, the heavy neutral leptons can decay into final states consisting of lighter mesons and leptons. In this section, we explain how we obtain the relevant decay rates.

A.1 Charged currents — two-body final states

When calculating decay rates involving an external meson, hadronic matrix elements between the meson and the quark currents must be evaluated. When the decay only involves a single external meson, such matrix elements are parameterized with decay constants. For a charged

JHEP01(2024)108

pseudoscalar meson M_{ij} with mass m_M consisting of the anti-quark $\bar{q}_i$ and quark q_j exist two non-zero quark-connections defined as

$$\langle 0 \,|\, \bar{q}_i \gamma^\mu \gamma_5 q_j \,|\, M_{ij}(p) \rangle = i p^\mu f_M \,, \tag{A.1}$$

$$\langle 0 \,|\, \bar{q}_i \gamma_5 q_j \,|\, M_{ij}(p) \rangle = i f_M^{PS} \,, \tag{A.2}$$

where p^μ is the momentum of the meson M_{ij}. Both decay constants f_M and f_M^{PS} are related via quark current algebra

$$-i \frac{m_M^2}{m_{\bar{q}_i} + m_{q_j}} f_M \equiv i f_M^{PS} \,. \tag{A.3}$$

Similarly, we define two decay constants for a charged vector meson M_{ij}^* with mass m_{M^*}, momentum p^μ and polarization ϵ^ν via

$$\langle 0 \,|\, \bar{q}_i \gamma^\mu q_j \,|\, M_{ij}^*(p,\epsilon) \rangle = m_{M^*} \epsilon^\mu f_{M^*} \,, \tag{A.4}$$

$$\langle 0 \,|\, \bar{q}_i \sigma^{\mu\nu} q_j \,|\, M_{ij}^*(p,\epsilon) \rangle = i(p^\mu \epsilon^\nu - p^\nu \epsilon^\mu) f_{M^*}^T \,, \tag{A.5}$$

where $\sigma^{\mu\nu} = \frac{i}{2}[\gamma^\mu, \gamma^\nu]$. In the heavy quark limit, we can relate both vector meson decay constants via $f_{M^*}^T \approx f_{M^*}$.

Employing these matrix elements we can evaluate the spin-averaged squared matrix elements $|\mathcal{M}|^2$ and obtain the decay rates for a process $P1 \to P2 + P3$. With the spin-averaging factor n for particle $P1$ and the respective masses m_1, m_2 and m_3 the decay rates are given by

$$\Gamma = \frac{\sqrt{\lambda(m_1^2, m_2^2, m_3^2)}}{16\pi m_1^3} \frac{1}{n} \sum_{\text{spins}} |\mathcal{M}|^2 \,, \tag{A.6}$$

where $\lambda(a,b,c) = a^2 + b^2 + c^2 - 2ab - 2ac - 2bc$ is the Källén function.

The spin-averaged squared matrix elements for a charged pseudoscalar meson $M_{ij}^\pm \to l_k^\pm + N$ in terms of the most general couplings in eq. (2.6) is given by[11]

$$\begin{aligned}
\sum_{\text{spins}} |\mathcal{M}(M_{ij}^\pm \to l_k^\pm + N)|^2 = \frac{G_F^2}{2} \Big\{ & f_M^2 \Big[|2V_{ij}U_{k4}|^2 + |c_{\text{VLR},ijk}^{CC1} - c_{\text{VRR},ijk}^{CC}|^2 \Big] \lambda_{V1} \\
& + f_M^2 \text{Re}[2V_{ij}U_{k4}(c_{\text{VLR},ijk}^{CC1} - c_{\text{VRR},ijk}^{CC})^*] \lambda_{V2} \\
& + (f_M^{PS})^2 |c_{\text{SLR},ijk}^{CC} - c_{\text{SRR},ijk}^{CC}|^2 \lambda_S \\
& + f_M f_M^{PS} \text{Re}[2V_{ij}U_{k4}(c_{\text{SLR},ijk}^{CC} - c_{\text{SRR},ijk}^{CC})^*] \lambda_{SV1} \\
& + f_M f_M^{PS} \text{Re}[(c_{\text{VLR},ijk}^{CC1} - c_{\text{VRR},ijk}^{CC})(c_{\text{SLR},ijk}^{CC} - c_{\text{SRR},ijk}^{CC})^*] \lambda_{SV2} \Big\}
\end{aligned} \tag{A.7}$$

[11] These decay rates have been calculated in appendix A of ref. [45], but we observe some differences. On one hand, we do not explicitly rotate to the neutrino mass basis, but instead assume, that mixing is minimal and hence $\nu_4 \approx \nu_R$. This also means, that we do not express the coupling for the interaction $(\bar{u}_L \gamma^\mu d_L)(\bar{e}_L \gamma_\mu \nu_L)$ with a Wilson coefficient c_{VLL}^{CC}, but instead only state the SM contribution $-2V_{ij}$, which changes the signs of some mass function λ and λ' in the interference terms. Additionally, because we use a different definition for the decay constants for vector mesons M^*, the sign of some interference terms for the decay mode $N \to l_k^\pm + M_{ji}^{*\mp}$ changes relative to ref. [45]. However, the Wilson coefficients could in principle be chosen to be negative, so that the sign of interference is a matter of convention.

JHEP01(2024)108

where we define the mass terms

$$\begin{aligned}
\lambda_{V1} &= m_M^2(m_N^2 + m_l^2) - (m_N^2 - m_l^2)^2\,, \\
\lambda_{V2} &= 4m_M^2 m_N m_l\,, \\
\lambda_S &= m_M^2 - m_N^2 - m_l^2\,, \\
\lambda_{SV1} &= 2m_N(m_M^2 - m_N^2 + m_l^2)\,, \\
\lambda_{SV2} &= 2m_l(m_M^2 + m_N^2 - m_l^2)\,,
\end{aligned} \tag{A.8}$$

where m_l and m_N are the masses of the lepton and N, respectively. If the initial meson is a vector meson, the most general spin-averaged squared matrix element is

$$\begin{aligned}
\frac{1}{3}\sum_{\text{spins}} |\mathcal{M}(M_{ij}^{*\pm} \to l_k^\pm + N)|^2 = \frac{G_F^2}{6}\Big\{ & f_{M^*}^2\Big[|2V_{ij}U_{k4}|^2 + |c_{\text{VLR},ijk}^{CC1} + c_{\text{VRR},ijk}^{CC}|^2\Big]\lambda'_{V1} \\
& + f_{M^*}^2 \text{Re}[2V_{ij}U_{k4}(c_{\text{VLR},ijk}^{CC1} + c_{\text{VRR},ijk}^{CC})^*]\lambda'_{V2} \\
& + (f_{M^*}^T)^2 |c_{\text{T},ijk}^{CC}|^2 \lambda'_T \\
& + f_{M^*} f_{M^*}^T \text{Re}[2V_{ij}U_{k4} c_{\text{TRR},ijk}^{CC,*}]\lambda'_{VT1} \\
& + f_{M^*} f_{M^*}^T \text{Re}[(c_{\text{VLR},ijk}^{CC1} + c_{\text{VRR},ijk}^{CC}) c_{\text{TRR},ijk}^{CC,*}]\lambda'_{VT2}\Big\},
\end{aligned} \tag{A.9}$$

where we define the mass terms

$$\begin{aligned}
\lambda'_{V1} &= m_{M^*}^2(2m_{M^*}^2 - m_N^2 - m_l^2) - (m_N^2 - m_l^2)^2\,, \\
\lambda'_{V2} &= -12m_{M^*}^2 m_N m_l\,, \\
\lambda'_T &= 16\Big(m_{M^*}^2(m_{M^*}^2 + m_N^2 + m_l^2) - 2(m_N^2 - m_l^2)^2\Big)\,, \\
\lambda'_{VT1} &= 24m_{M^*} m_N(m_{M^*}^2 - m_N^2 + m_l^2)\,, \\
\lambda'_{VT2} &= -24m_{M^*} m_l(m_{M^*}^2 + m_N^2 - m_l^2)\,.
\end{aligned} \tag{A.10}$$

For an LLNF decaying into a meson and a lepton, we can relate the spin-averaged squared matrix element to the squared matrix element of an identical meson decaying into an N and identical lepton. Including the charge-conjugate decay modes and appropriate spin-averaging factors, we find

$$2 \times \frac{1}{2}\sum_{\text{spins}} |\mathcal{M}(N \to l_k^\pm + M_{ij}^{(*)\mp})|^2 = -\sum_{\text{spins}} |\mathcal{M}(M_{ij}^{(*)\pm} \to l_k^\pm + N)|^2. \tag{A.11}$$

A.2 Neutral currents — two-body final states

If the meson involved in the decay modes are charge-neutral, the contributing couplings are given in eq. (2.7). The resulting modes are $M_{ij}^0 \to \nu_k + N$ and $N \to \nu_k + M_{ji}^0$. However, as neutral mesons do not always correspond to a single $\bar{q}_i q_j$ state, we must treat the hadronic matrix element differently based on the involved meson. We divide the mesons into heavy neutral mesons (involving a charm or bottom quark), kaons, and other light neutral mesons.

JHEP01(2024)108

A.2.1 Heavy neutral mesons

Heavy neutral mesons such as D^0, B^0, B_s^0 and the related vector mesons do correspond to a pure $\bar{q}_i q_j$ state, so that we can define the decay constants similarly to eqs. (A.1)–(A.5). As the quark currents must be flavor-changing to allow for these decays, only the three neutral EFT-couplings contribute to the decay modes. For a neutral heavy pseudoscalar mesons, we find

$$\sum_{\text{spins}} |\mathcal{M}(M_{ij}^0 \to \nu_k + N)|^2 = \frac{G_F^2}{2} (f_M^{PS})^2 |c_{\text{SLR},ijk}^{NC} - c_{\text{SRR},ijk}^{NC}|^2 \lambda_S \,, \tag{A.12}$$

$$2 \times \frac{1}{2} \sum_{\text{spins}} |\mathcal{M}(N \to \nu_k + M_{ij}^0)|^2 = - \sum_{\text{spins}} |\mathcal{M}(M_{ij}^0 \to \nu_k + N)|^2 \,.$$

Similarly, for a heavy neutral vector meson the spin-averaged matrix element squared is

$$\frac{1}{3} \sum_{\text{spins}} |\mathcal{M}(M_{ij}^{0*} \to \nu_k + N)|^2 = \frac{G_F^2}{6} (f_M^T)^2 |c_{\text{T},ijk}^{NC}|^2 \lambda_T' \,, \tag{A.13}$$

$$2 \times \frac{1}{2} \sum_{\text{spins}} |\mathcal{M}(N \to \nu_k + M_{ij}^{0*})|^2 = - \sum_{\text{spins}} |\mathcal{M}(M_{ij}^{0*} \to \nu_k + N)|^2 \,.$$

A.2.2 Kaons

Neutral pseudoscalar kaons K^0 ($\bar{s}d$) and $\bar{K}^0$ ($\bar{d}s$) are flavor eigenstates and can be produced in strong interactions, while their decay implies change of flavor and occurs via weak interactions. However, both are not eigenstates of weak interactions. Knowing that

$$\hat{CP} \left| K^0 \right\rangle = - \left| \bar{K}^0 \right\rangle \,, \tag{A.14}$$

$$\hat{CP} \left| \bar{K}^0 \right\rangle = - \left| K^0 \right\rangle \,, \tag{A.15}$$

we define the following CP eigenstates (which are simultaneous eigenstates for the total Hamiltonian assuming no CP violation)

$$|K_1\rangle = \frac{1}{\sqrt{2}} \left(\left| K^0 \right\rangle - \left| \bar{K}^0 \right\rangle \right) , \qquad \text{with } \hat{CP} |K_1\rangle = |K_1\rangle \,, \tag{A.16}$$

$$|K_2\rangle = \frac{1}{\sqrt{2}} \left(\left| K^0 \right\rangle + \left| \bar{K}^0 \right\rangle \right) , \qquad \text{with } \hat{CP} |K_2\rangle = - |K_2\rangle \,. \tag{A.17}$$

The actual physical kaons K_L and K_S are, however, not CP eigenstates, but violate CP slightly. They are mixtures of $K_{1/2}$. We can parameterize this mixture with a parameter $\epsilon \sim \mathcal{O}(10^{-3})$ and obtain

$$|K_S\rangle = \frac{1}{\sqrt{(1+\epsilon^2)}} \Big[|K_1\rangle + \epsilon |K_2\rangle \Big] \,, \tag{A.18}$$

$$|K_L\rangle = \frac{1}{\sqrt{(1+\epsilon^2)}} \Big[|K_2\rangle + \epsilon |K_1\rangle \Big] \,. \tag{A.19}$$

JHEP01(2024)108

In practice, we will interpret $\left|K_{S/L}\right\rangle = \left|K_{1/2}\right\rangle$ and ignore the CP violation (assuming $\epsilon \to 0$). Then, we have the following decay constants for kaons

$$\begin{aligned}\left\langle 0 \left| \bar{d}\gamma^\mu\gamma_5 s \right| K_{L/S}(p)\right\rangle &= \pm\frac{i}{\sqrt{2}} p^\mu f_{K^0}\,,\\ \left\langle 0 \left| \bar{s}\gamma^\mu\gamma_5 d \right| K_{L/S}(p)\right\rangle &= \frac{i}{\sqrt{2}} p^\mu f_{K^0}\,.\end{aligned} \tag{A.20}$$

As such decay modes necessitate flavor changing quark currents, only the EFT couplings of eq. (2.7) contribute and the squared matrix element is given by eq. (A.12) adjusted for the additional factor $1/\sqrt{2}$.

Neutral vector kaons are flavor eigenstates as well as physically propagating states, so that we can use the expression eq. (A.13) for such decay modes.

A.2.3 Light neutral mesons

Light neutral mesons are mixtures of quark-antiquark pairs. The decay constants as defined in eqs. (A.1)–(A.5), however, connect to a quark current consisting of a single quark-antiquark pair. We can relate the relevant hadronic matrix element to the matrix element of the associated charged meson using G-parity and isospin relations.[12] G-Parity is a multiplicative quantum number combining the charge conjugation and an isospin rotation along the second axis and is conserved by strong interactions.

$$\hat{G} = \hat{C}\hat{R}_2 = \hat{C}\exp(i\pi\hat{I}_2)\,. \tag{A.21}$$

Pions and the ω-meson are G-parity odd, while ρ-mesons are G-parity even. The quark currents involving only light mesons, u und d can be constructed with quark currents, which are also eigenstates of G-parity. For example, the down-type axial-vector current is a mix of the G-parity even $j_\mu^{A,s}$ and the G-parity odd $j_\mu^{A,0}$

$$\begin{aligned} j_\mu^{A,s} &= \frac{1}{\sqrt{2}}(\bar{u}\gamma_\mu\gamma_5 u + \bar{d}\gamma_\mu\gamma_5 d)\,,\\ j_\mu^{A,0} &= \frac{1}{\sqrt{2}}(\bar{u}\gamma_\mu\gamma_5 u - \bar{d}\gamma_\mu\gamma_5 d)\,,\\ \bar{d}\gamma_\mu\gamma_5 d &= \frac{1}{\sqrt{2}}(j_\mu^{A,s} - j_\mu^{A,0})\,.\end{aligned} \tag{A.22}$$

Assuming G-parity symmetry, we can relate matrix elements for light neutral mesons and light charged mesons. Here, we assume ideal mixing between ω and ϕ. In such a case ϕ is a pure $\bar{s}s$-state. Lastly, matrix elements for quark currents involving external η and η' must be handled more carefully. Both are neutral unflavored mesons with zero isospin involving the axial singlet state ϕ^0. Because ϕ^0 is involved, the anomaly of the axial-vector singlet current affects η-η' mixing significantly. To account for these effects, we adopt an extended two-parameter mixing scheme as proposed in refs. [84, 163, 164]. If we denote light up-type and down-type quarks u and d as q_l, the decay constants are defined via[13]

[12] We follow appendix B of ref. [120].

[13] The extension of the two-angle mixing scheme by splitting the contributions to the isospin doublet (u, d) and strange contributions was incentivized by the observation that chiral symmetry breaking effects differ because of the larger s-mass.

JHEP01(2024)108

f_8/f_π	f_1/f_π	θ^8	θ^1
1.26	1.17	-0.37 rad	-0.16 rad

Table 12. Phenomenological values to determine decay constants for η and η' [164].

$$\langle 0 | \bar{q}_l \gamma^\mu \gamma_5 q_l | \eta^{(\prime)}(p) \rangle = i p^\mu f_{\eta^{(\prime)}}^{\bar{q}_l q_l}, \tag{A.23}$$

$$\langle 0 | \bar{s} \gamma^\mu \gamma_5 s | \eta^{(\prime)}(p) \rangle = i p^\mu f_{\eta^{(\prime)}}^{\bar{s}s}, \tag{A.24}$$

and can be expressed in terms of the mixing parameters f^0, f^8, θ^0, and θ^8 as[14]

$$f_\eta^{\bar{q}_l q_l} = \frac{1}{\sqrt{3}} \left[- f_1 \sin\theta^1 + \frac{1}{\sqrt{2}} f_8 \cos\theta^8 \right], \qquad f_\eta^{\bar{s}s} = \frac{1}{\sqrt{3}} \left[- f_1 \sin\theta^1 - \sqrt{2} f_8 \cos\theta^8 \right], \tag{A.25}$$

$$f_{\eta'}^{\bar{q}_l q_l} = \frac{1}{\sqrt{3}} \left[f_1 \cos\theta^1 + \frac{1}{\sqrt{2}} f_8 \sin\theta^8 \right], \qquad f_{\eta'}^{\bar{s}s} = \frac{1}{\sqrt{3}} \left[f_1 \cos\theta^1 - \sqrt{2} f_8 \sin\theta^8 \right]. \tag{A.26}$$

Phenomenological values for all η-η' mixing-parameters are provided in table 12.

A.3 Three body final states

Other possible decay modes involve two external mesons, a lepton l, and the N. The relevant hadronic matrix element for such decays are parameterized with form factors, which are functions of the squared momentum transfer q^2. The q^2-dependence is typically calculated in a suited framework (e.g. lattice QCD or constituent quark models), the results of which are fitted to a parameterization formula. The number of required form factors depends on the number of independent Lorentz covariant structures formed by the available Lorentz vectors. For the decay of a pseudoscalar meson M to a final state involving a pseudoscalar meson M',the set of form factors required to describe the occurring matrix elements are

$$\left\langle M'(p') \middle| \bar{q}_1 q_2 \middle| M(p) \right\rangle = f_S(q^2), \tag{A.27}$$

$$\begin{aligned} \left\langle M'(p') \middle| \bar{q}_1 \gamma^\mu q_2 \middle| M(p) \right\rangle &= f_+(q^2) P^\mu + f_-(q^2) q^\mu \\ &= f_+(q^2) \left(P^\mu - \frac{m_M^2 - m_{M'}^2}{q^2} q^\mu \right) + f_0(q^2) \frac{m_M^2 - m_{M'}^2}{q^2} q^\mu, \end{aligned} \tag{A.28}$$

$$\left\langle M'(p') \middle| \bar{q}_1 \sigma^{\mu\nu} q_2 \middle| M(p) \right\rangle = \frac{2i}{m_M + m_{M'}} (p^\mu p'^\nu - p^\nu p'^\mu) f_T(q^2), \tag{A.29}$$

where $P^\mu = p^\mu + p'^\mu$ and $q^\mu = p^\mu - p'^\mu$ and

$$f_0(q^2) = f_+(q^2) + \frac{q^2}{m_M^2 - m_{M'}^2} f_-(q^2). \tag{A.30}$$

As the SM does not include tensor currents, f_T-parameterizations are only present for some meson combinations M-M', but we can relate $f_S(q^2)$ and $f_T(q^2)$ to the form factors of the

[14] In $f_{\eta/\eta'}^{\bar{q}_l q_l}$ we apply an additional factor $1/\sqrt{2}$, as the neutral axial current consists only of u or d.

JHEP01(2024)108

vector current via current-algebra as

$$f_S(q^2) = f_0(q^2)\frac{m_M^2 - m_{M'}^2}{m_{q_2} - m_{\bar{q}_1}}, \tag{A.31}$$

$$f_T(q^2) \simeq \frac{m_M(m_M + m_{M'})}{q^2}[f_+(q^2) - f_0(q^2)]. \tag{A.32}$$

We find that eq. (A.32) agrees reasonably well for known f_T- parameterizations [165–167]. We assume the approximation to be justified and apply eq. (A.32) to describe tensor form factors of meson pairs, where they are unknown.

If M' is a vector meson, there exist four hadronic matrix elements.

$$\left\langle M'^*(p',\epsilon)\left|\,\bar{q}_1\gamma_5 q_2\,\right|M(p)\right\rangle = if_{PS}(q^2)(\epsilon^*\cdot p), \tag{A.33}$$

$$\left\langle M'^*(p',\epsilon)\left|\,\bar{q}_1\gamma^\mu q_2\,\right|M(p)\right\rangle = g(q^2)\epsilon^{\mu\nu\alpha\beta}\epsilon^*_\nu p_\alpha p'_\beta, \tag{A.34}$$

$$\left\langle M'^*(p',\epsilon)\left|\,\bar{q}_1\gamma^\mu\gamma_5 q_2\,\right|M(p)\right\rangle = i\Big[a_+(q^2)P^\mu(\epsilon^*\cdot p) + a_-(q^2)q^\mu(\epsilon^* p) + f(q^2)\epsilon^{*\mu}\Big], \tag{A.35}$$

$$\left\langle M'^*(p',\epsilon)\left|\,\bar{q}_1\sigma^{\mu\nu} q_2\,\right|M(p)\right\rangle = i\epsilon^{\mu\nu\alpha\beta}\Big[g_+(q^2)\epsilon^*_\alpha P_\beta + g_-(q^2)\epsilon^*_\alpha q_\beta + g_0(q^2)p_\alpha p'_\beta(\epsilon^*\cdot p)\Big]. \tag{A.36}$$

Again, f_{PS} can be related to the axial-vector current formfactors via current-algebra via

$$f_{PS}(q^2) = -\frac{1}{(m_{\bar{q}_1} + m_{q_2})}\Big[a_+(q^2)(m_M^2 - m_{M'}^2) + a_-(q^2)q^2 + f(q^2)\Big]. \tag{A.37}$$

The parameterizations for form factors are usually stated as the mode $M \to M'$, where charges are not assigned. However, as is the case for decay constants of kaons and other light mesons, we can relate the hadronic matrix elements between various possible modes using isospin symetry. As an example for a decay of the type $D \to \pi$ with the general Dirac matrix element Γ, we find

$$\left\langle \pi^0\left|\,\bar{u}\Gamma c\,\right|D^0\right\rangle = \frac{1}{\sqrt{2}}\left\langle \pi^+\left|\,\bar{u}\Gamma c\,\right|D^+\right\rangle = \frac{1}{\sqrt{2}}\left\langle \pi^-\left|\,\bar{d}\Gamma c\,\right|D^0\right\rangle = -\left\langle \pi^0\left|\,\bar{d}\Gamma c\,\right|D^0\right\rangle. \tag{A.38}$$

We observe that the relative matrix elements may differ in sign and in a factor $1/\sqrt{2}$ for every external π^0, ρ^0 or $K_{L/S}$.

Equipped with all possible form factors, we can calculate the decay rate of a semi-leptonic meson decay. This involves lengthy three-body phase-space calculations and can not always be done analytically. Instructions on how to perform the computations numerically with the help of `Mathematica` are provided in appendix B of ref. [45].

B Phenomenological values

In this section, we list the phenomenological values used in this paper. This includes specific SM decay constants, and form factors. For the CKM-matrix elements, the renormalized

JHEP01(2024)108

M	f_M [MeV]	Ref.	M^*	f_{M^*} [MeV]	Ref.
π	130.2	[168]	ρ	209.4	[111, 169, 170]
K	155.7	[168]	K^*	205.7	[111, 169, 170]
η - $\bar{q}q$	76.5	[84, 164]	ω	201.1	[111, 169, 170]
η - $\bar{s}s$	-110.8	[84, 164]	ϕ	228.1	[111, 169, 170]
η' - $\bar{q}q$	62.6	[84, 164]			
η' - $\bar{s}s$	135.3	[84, 164]			
D	212.0	[168]	D^*	212.0	[168]
D_s	249.9	[168]	D^*	249.9	[168]
B	190.0	[168]	B^*	190.0	[168]
B_s	230.3	[168]	B_s^*	230.3	[168]
η_c	387.0	[171]	J/ψ	418.0	[171]

Table 13. Decay constants for pseudoscalar and vector mesons defined in eqs. (A.2) and (A.1).

quark-masses, and other particle masses, we follow the latest results of the Particle Data Group (PDG [111]). The currently stated values for the CKM elements are

$$\begin{aligned} |V_{ud}| &= 0.97373, & |V_{us}| &= 0.2243, & |V_{ub}| &= 3.82 \times 10^{-3}, \\ |V_{cd}| &= 0.221, & |V_{cs}| &= 0.975, & |V_{cb}| &= 40.8 \times 10^{-3}. \end{aligned} \tag{B.1}$$

The quark masses renormalized with the $\overline{\text{MS}}$ renormalization scheme at the scale $\mu = 2\,\text{GeV}$ are

$$\begin{aligned} m_u &= 2.16\,\text{MeV}, & m_c &= 1.27\,\text{GeV}, & \\ m_d &= 4.67\,\text{MeV}, & m_s &= 93.4\,\text{MeV}, & m_b &= 4.18\,\text{GeV}. \end{aligned} \tag{B.2}$$

B.1 Decay constants

Here, we state the numerical values used for the decay constants defined in eqs. (A.1)–(A.5). For pseudoscalar decay constants we rely on the most recent `FLAG` review [168] and the parameterization of ref. [164]. For charmed and bottomed vector mesons we employ the heavy-quark limit approximation $f_{M'} = f_M$. For light vector mesons, we can calculate the decay constants as described in refs. [169, 170]. The numerical values of all decay constants are listed in table 13.

B.2 Form factor parameterizations

Next, we state the form factor parameterizations that we use for the various decay modes involving an incoming pseudoscalar M and an outgoing M' with respective masses m_M and $m_{M'}$. The parameterizations are stated for a charged quark current, which we then relate to all other charge assignments as described in section A.3. It is common to expand the

JHEP01(2024)108

Form factor	$M \to M'$	$f(0)$	λ
$f_+(q^2)$	$K^\pm \to \pi^0$	0.9698	0.0277
$f_0(q^2)$	$K^\pm \to \pi^0$	0.9698	0.0183
$f_+(q^2)$	$K^0 \to \pi^\pm$	0.9698	0.0267
$f_0(q^2)$	$K^0 \to \pi^\pm$	0.9698	0.0117

Table 14. Form factor fit parameters of $K \to \pi$ using the parameterization of eq. (B.8) [120, 168, 173, 174].

form factors in terms of a dimensionless variable $z(q^2)$ defined as

$$z(q^2) \equiv \frac{\sqrt{t_+ - q^2} - \sqrt{t_+ - t_0}}{\sqrt{t_+ - q^2} + \sqrt{t_+ - t_0}}\,. \tag{B.3}$$

We follow the FLAG collaboration [168] in writing t_+ and t_0 as

$$t_\pm = (m_M \pm m_{M'})^2, \tag{B.4}$$

$$t_0 = t_+\left[1 - \sqrt{1 - \frac{t_-}{t_+}}\right] = (m_M + m_{M'})\left(\sqrt{m_M} - \sqrt{m_{M'}}\right)^2. \tag{B.5}$$

B.2.1 Kaons: $K \to \pi$

The scalar and vector form factors for $K \to \pi$ are described reasonably well by a linear q^2-dependence of the form

$$f(q^2) = f(0) \cdot \left(1 + \lambda \frac{q^2}{m_{\pi^+}^2}\right). \tag{B.6}$$

The optimal fit parameters for this parameterization are listed in table 14. For the tensor form factor, we follow ref. [172] and use a pole-parameterization

$$f_T(q^2) = \frac{f_T(0)}{1 - s_T\, q^2}\,, \tag{B.7}$$

where $f_T(0) = 0.417$ and $s_T = 1.10\,\mathrm{GeV}^{-2}$.

B.2.2 Charmed mesons: $D \to \pi/K$

The ETM Collaboration has recently published results for the form factors $f_{+,0,T}(q^2)$ [165, 175] in the form

$$f(q^2) = \frac{f(0) + c(z(q^2) - z_0)\left(1 + \frac{z(q^2)+z_0}{2}\right)}{1 - Pq^2}, \tag{B.8}$$

where $z_0 = z(q^2 = 0)$. The fitted results for $f(0)$, c and P are listed in table 15.

JHEP01(2024)108

Form factor	$M \to M'$	$f(0)$	c	P [GeV^{-2}]
$f_+(q^2)$	$D \to \pi$	0.6117	-1.985	0.1314
$f_0(q^2)$	$D \to \pi$	0.6117	-1.188	0.0342
$f_T(q^2)$	$D \to \pi$	0.5063	-1.10	0.1461
$f_+(q^2)$	$D \to K$	0.7647	-0.066	0.2241
$f_0(q^2)$	$D \to K$	0.7647	-2.084	0
$f_T(q^2)$	$D \to K$	0.6871	-2.86	0.0854

Table 15. Form factor fit parameters of $D \to \pi, K$ using the parameterization of eq. (B.8) [165, 175].

Form factor	$M \to M'$	$f(0)$	σ_1	σ_2
$f_+(q^2)$	$D_s \to \eta$	0.78	0.69	0.002
$f_-(q^2)$	$D_s \to \eta$	-0.42	0.74	0.008
$f_+(q^2)$	$D_s \to \eta'$	0.73	0.88	0.018
$f_-(q^2)$	$D_s \to \eta'$	-0.28	0.92	0.009
$f_+(q^2)$	$D_s \to K$	0.60	1.05	0.18
$f_-(q^2)$	$D_s \to K$	-0.38	1.14	0.24

Table 16. Form factor fit parameters of $D_s \to \eta, \eta', K$ using the parameterization of eq. (B.9) [176].

B.2.3 Charmed strange mesons: $D_s \to \eta/\eta'/K$

For the decay channels $D_s \to \eta, \eta', K$, we apply a double-pole parameterization used in ref. [176] of the form

$$f(q^2) = \frac{f(0)}{1 - \sigma_1 \frac{q^2}{m_{D_s}^2} + \sigma_2 \frac{q^4}{m_{D_s}^4}}. \tag{B.9}$$

To take η-η' mixing into account, the authors of ref. [176] follow the same scheme as used in ref. [164], which we also employ for the decay constants for η-η'. The fit parameters are summarized in table 16.

B.2.4 Bottom mesons: $B \to \pi/K/D$ and $B_s \to K/D_s$

The FLAG collaboration [168] presents form factors using the z-expansion proposal by Bourrely, Caprini, and Lellouch (BCL)

$$f_{+,T}(q^2) = \frac{1}{1 - \frac{q^2}{M_{+,T}^2}} \sum_{n=0}^{N-1} a_n^{+,T} \left[z^n - (-1)^{n-N} \frac{n}{N} z^N \right], \tag{B.10}$$

$$f_0(q^2) = \frac{1}{1 - \frac{q^2}{M_0^2}} \sum_{n=0}^{N-1} a_n^0 z^n. \tag{B.11}$$

JHEP01(2024)108

$M \to M'$	N	M_+ [GeV]	a_0^+	a_1^+	a_2^+	a_3^+	M_0 [GeV]	a_0^0	a_1^0	a_2^0
$B \to \pi$	3	5.32465	0.404	-0.68	-0.86	/	∞	0.49	-1.61	/
$B \to K$	3	5.4154	0.471	-0.74	0.32	/	5.711	0.301	0.40	/
$B \to D$	3	∞	0.896	-7.94	51.4	/	∞	0.7821	-3.28	/
$B_s \to K$	4	5.32465	0.374	-0.672	0.07	1.34	5.68	0.2203	0.089	0.24
$B_s \to D_s$	3	6.329	-0.075	-3.24	0.7	/	6.704	0.666	-0.26	-0.1

Table 17. Vector and scalar form factor fit parameters for the transitions $B \to \pi$, $B_{(s)} \to K$, and $B_{(s)} \to D_{(s)}$ using the parameterization of eq. (B.10) and eq. (B.11) [168, 177, 178].

$M \to M'$	N	M_T [GeV]	a_0^T	a_1^T	a_2^T	a_3^T
$B \to \pi$	4	5.32465	0.393	-0.65	-0.6	0.1
$B \to K$	3	5.4154	0.455	-1.00	-0.9	/

Table 18. Tensor form factor fit parameters for the transitions $B \to \pi$ and $B \to K$ using the parameterization of eq. (B.10) [168, 177, 179].

For f_0 one coefficient a_n is restricted by imposing $f_+(0) = f_0(0)$, so that

$$a_{N-1}^0 = \frac{1}{z^{N-1}(0)}\left[f_+(0) - \sum_{n=0}^{N-2} a_n^0 z^n(0)\right]. \tag{B.12}$$

Optimal fit values are stated in table 17. For the decay modes $B_s \to K$, t_+ and t_- are not defined for the same meson masses. Instead, both functions are defined as $t_+ = (m_B + m_\pi)^2$ and $t_- = (m_{B_s} + m_K)^2$, respectively. For $B_s \to D_s$, the dimensionless variable $z(q^2)$ is defined for $t_0 = 0$.

B.2.5 Bottom strange meson decays $B_s \to \eta^{(\prime)}$

Such a decay mode is mediated by the $b \to s$ quark current. However, the $\eta^{(\prime)}$ final state is a mixture of light and strange quarks. As was the case for decay constants, we must account for strange component in the final state meson. We follow ref. [167] and calculate the decay rates as

$$\Gamma(D_s \to \eta + l + \nu) = \sin^2(\theta)\Gamma(D_s \to \eta_s(M_\eta) + l + \nu)\,, \tag{B.13}$$

$$\Gamma(D_s \to \eta' + l + \nu) = \cos^2(\theta)\Gamma(D_s \to \eta_s(M_{\eta'}) + l + \nu)\,, \tag{B.14}$$

where $\theta \approx 40^\circ$. The parameterizations of the form factors of a hadronic matrix element of the form $\langle \eta_s(M_{\eta^{(\prime)}})|b\Gamma s|B_s\rangle$ is then given by

$$f_{+,T}(q^2) = \frac{f(q^2)}{\left(1 - \frac{q^2}{M^2}\right)\left[1 - \sigma_1 \frac{q^2}{M^2} + \sigma_2 \frac{q^4}{M^4}\right]}\,, \tag{B.15}$$

$$f_0(q^2) = \frac{f(q^2)}{\left[1 - \sigma_1 \frac{q^2}{M^2} + \sigma_2 \frac{q^4}{M^4}\right]}\,. \tag{B.16}$$

The parameters for both decays are stated in table 19.

JHEP01(2024)108

Fit Parameters	f_+	f_0	f_T	Fit Parameters	f_+	f_0	f_T
$[B_s \to \eta_s(M_\eta)]$				$[B_s \to \eta_s(M_{\eta'})]$			
$f(0)$	0.36	0.36	0.36	$f(0)$	0.36	0.36	0.39
σ_1	0.60	0.80	0.58	σ_1	0.60	0.80	0.58
σ_2	0.20	0.40	0.18	σ_2	0.20	0.45	0.18
M [GeV]	5.42	5.42	5.42	M [GeV]	5.42	5.42	5.42

Table 19. Vector and tensor form factor fit parameters of $B_s \to \eta_s(M_{\eta^{(\prime)}})$.

B.2.6 Final state vector mesons

If M' is a vector meson, we also refer to the form factor parameterizations in ref. [167]. There, parameterizations are provided for linear combinations of the form factors defined in eqs. (A.33)–(A.36) These linear combinations are defined as

$$\begin{aligned} V =&(m_M + m_{M'})g\,, \\ A_0 =&\frac{1}{2m_{M'}}(f + q^2 \cdot a_- + (m_M^2 - m_{M'}^2)a_+)\,, \qquad & T_1 =& -g_+\,, \\ A_1 =&\frac{1}{m_M + m_{M'}}f\,, & T_2 =& -g_+ - \frac{q^2}{m_M^2 - m_{M'}^2}g_-\,, \\ A_2 =& -(m_M + m_{M'})a_+\,, & T_3 =& g_- - \frac{m_M^2 - m_{M'}^2}{2}g_0\,. \end{aligned} \tag{B.17}$$

From eq. (A.37), we also see that

$$A_0 = -\frac{m_{\bar{q}_1} + m_{q_2}}{2M_2}f_{PS}\,. \tag{B.18}$$

The parameterization used for these new variables is similar to eq. (B.9), where M_{D_s} is modified for every decay mode. For F_+, F_T, V, T_1, and A_0, resonances contribute strongly to the behavior of the form factor. To accurately include the influence of such resonances, the fit-function is adjusted to

$$f(q^2) = \frac{f(q^2)}{\left(1 - \frac{q^2}{M^2}\right)\left[1 - \sigma_1\frac{q^2}{M^2} + \sigma_2\frac{q^4}{M^4}\right]}. \tag{B.19}$$

Detailed in table 20 and table 21 are the relevant fit parameters for a final state vector meson.

C RPV derivation

In this section, we perform the derivation of the 4-fermion vertex interactions in the context of R-parity violating supersymmetry.[15] The resulting dimension-6 operators can be matched

[15]We follow the procedure described in ref. [92]. However, instead of using four-component Dirac spinors, we employ the two-component Weyl spinor notation used in ref. [180]. Further, we correct an erroneous factor in the Fierz-identity in ref. [92].

JHEP01(2024)108

Fit Parameters	V	A_0	A_1	A_2	T_1	T_2	T_3
$[B \to \rho]$							
$f(0)$	0.31	0.30	0.26	0.24	0.27	0.27	0.19
σ_1	0.59	0.54	0.73	1.40	0.60	0.74	1.42
σ_2	0.00	0.00	0.10	0.50	0.00	0.19	0.51
M [GeV]	5.32	5.27	5.32	5.32	5.32	5.32	5.32
$[B \to K^*]$							
$f(0)$	0.44	0.45	0.36	0.32	0.39	0.39	0.27
σ_1	0.45	0.46	0.64	1.23	0.45	0.72	1.31
σ_2	0.0	0.0	0.36	0.38	0.0	0.62	0.41
M [GeV]	5.42	5.37	5.42	5.42	5.42	5.42	5.42
$[B \to D^*]$							
$f(0)$	0.76	0.69	0.66	0.62	0.68	0.68	0.33
σ_1	0.57	0.58	0.78	1.40	0.57	0.64	1.46
σ_2	0.0	0.0	0.0	0.41	0.0	0.0	0.50
M [GeV]	6.4	6.4	6.4	6.4	6.4	6.4	6.4
$[B_s \to K^*]$							
$f(0)$	0.38	0.37	0.29	0.26	0.32	0.32	0.23
σ_1	0.66	0.60	0.86	1.32	0.66	0.98	1.42
σ_2	0.30	0.16	0.60	0.54	0.31	0.90	0.62
M [GeV]	5.32	5.27	5.32	5.32	5.32	5.32	5.32
$[B_s \to \phi]$							
$f(0)$	0.44	0.42	0.34	0.31	0.38	0.38	0.26
σ_1	0.62	0.55	0.73	1.30	0.62	0.83	1.41
σ_2	0.20	0.12	0.42	0.52	0.20	0.71	0.57
M [GeV]	5.42	5.37	5.42	5.42	5.42	5.42	5.42

Table 20. Form factor fit parameters of $B_{(s)} \to M^*$ of the linear combinations of (B.17).

JHEP01(2024)108

Fit Parameters	V	A_0	A_1	A_2	T_1	T_2	T_3
$[D \to \rho]$							
$f(0)$	0.90	0.66	0.59	0.49	0.66	0.66	0.31
σ_1	0.46	0.36	0.50	0.89	0.44	0.38	1.10
σ_2	0.00	0.00	0.00	0.00	0.00	0.50	0.17
M [GeV]	2.01	1.87	2.01	2.01	2.01	2.01	2.01
$[D \to K^*]$							
$f(0)$	1.03	0.76	0.66	0.49	0.78	0.78	0.45
σ_1	0.27	0.17	0.30	0.67	0.25	0.02	1.23
σ_2	0.00	0.00	0.20	0.16	0.00	1.80	0.34
M [GeV]	2.11	1.97	2.11	2.11	2.11	2.11	2.11
$[D_s \to K^*]$							
$f(0)$	1.04	0.67	0.57	0.42	0.71	0.71	0.45
σ_1	0.24	0.20	0.29	0.58	0.22	-0.06	1.08
σ_2	0.00	0.00	0.42	0.00	0.00	0.44	0.68
M [GeV]	2.01	1.87	2.01	2.01	2.01	2.01	2.01
$[D_s \to \phi]$							
$f(0)$	1.10	0.73	0.64	0.47	0.77	0.77	0.46
σ_1	0.26	0.10	0.29	0.63	0.25	0.02	1.34
σ_2	0.00	0.00	0.00	0.00	0.00	2.01	0.45
M [GeV]	2.11	1.97	2.11	2.11	2.11	2.11	2.11

Table 21. Form factor fit parameters of $D_{(s)} \to M^*$ of the linear combinations of (B.17).

to the effective Lagrangian eq. (2.6) and eq. (2.7). We start with the chiral interactions in a supersymmetric extension of the Standard Model, which can be stated in terms of the superpotential W (For an in-depth discussion of supersymmetry, see e.g. refs. [180–182]). The most general form of the superpotential can be given as

$$W = W_{\text{MSSM}} + W_{\text{RPV}}\,, \tag{C.1}$$

$$W_{\text{MSSM}} = (y_u)_{ij} Q_i H_u \bar{u}_j - (y_d)_{ij} Q_i H_d \bar{d}_j - (y_l)_{ij} L_i H_d \bar{e}_j + \mu H_u H_d\,, \tag{C.2}$$

$$W_{\text{RPV}} = \kappa_i L_i H_u + \lambda_{ijk} L_i L_j \bar{e}_k + \lambda'_{ijk} L_i Q_j \bar{d}_k + \lambda''_{ijk} \bar{u}_i \bar{d}_j \bar{d}_k\,. \tag{C.3}$$

A minimal supersymmetric extension of the Standard Model (in terms of interactions) imposes a discrete $\mathbb{Z}_2$ symmetry, called R-parity. For a particle with baryon number B, lepton number

JHEP01(2024)108

L, and spin S, the R-parity is defined as $R_p = (-1)^{3(B-L)+2S}$. If R-parity is conserved, only the interactions of W_{MSSM} are allowed. If R-parity is violated, the interactions of W_{RPV}, which include three sets of lepton-number-violating and one set of baryon-number-violating terms, can also be non-zero. To still ensure the stability of the proton, we can, for example, impose a discrete $\mathbb{Z}_3$ symmetry, the baryon triality [183], so that the $\lambda'' \bar{u}\bar{d}\bar{d}$ terms are not allowed. Among the remaining three sets of lepton-number-violating operators, we are interested in the operators $\lambda' LQ\bar{d}$, which contribute to the decay of mesons. The interaction terms in component form are

$$\begin{aligned}\mathcal{L}_{\text{LQ}\bar{d}} = \lambda'_{ijk}\Big[&(e_i u_j)\widetilde{d}^*_{Rk} + (e_i \bar{d}_k)\widetilde{u}_{Lj} + (u_j \bar{d}_k)\widetilde{e}_{Li} \\ &- (\nu_i d_j)\widetilde{d}^*_{Rk} - (\nu_i \bar{d}_k)\widetilde{d}_{Lj} - (d_j \bar{d}_k)\widetilde{\nu}_{Li}\Big] + \text{h.c.}\,. \end{aligned} \tag{C.4}$$

The relevant supersymmetric gauge-interactions are given in component form by

$$\begin{aligned}\mathcal{L}_{\text{gauge}} \supset -\sqrt{2}g'\Big[&Y_L \widetilde{\nu}^*_{Li}(\nu_i \widetilde{\chi}^0_1) + Y_L \widetilde{e}^*_{Li}(e_i \widetilde{\chi}^0_1) \\ &+ Y_Q \widetilde{u}^*_{Lj}(u_j \widetilde{\chi}^0_1) + Y_Q \widetilde{d}^*_{Lj}(d_j \widetilde{\chi}^0_1) + Y_{\bar{d}} \widetilde{d}_{Rk}(\bar{d}_k \widetilde{\chi}^0_1)\Big] + \text{h.c.}\,. \end{aligned} \tag{C.5}$$

We assume the sfermion fields to be heavy ($\sim m_{\text{SUSY}}$) compared to the meson mass range (m_{QCD}). Hence below m_{SUSY}, we can integrate out the heavy degrees of freedom via the equation of motion. The resulting effective tree-level Lagrangian is given by

$$\begin{aligned}\mathcal{L} \supset \sqrt{2}g'\lambda'_{ijk}\Big[&\frac{Y_{\bar{d}}}{m^2_{\widetilde{d}_{Rk}}}\left[(\nu_i d_j)(\bar{d}_k \widetilde{\chi}^0_1) - (e_i u_j)(\bar{d}_k \widetilde{\chi}^0_1)\right] + \frac{Y_Q}{m^2_{\widetilde{d}_{Lj}}}(\nu_i \bar{d}_k)(d_j \widetilde{\chi}^0_1) \\ &- \frac{Y_Q}{m^2_{\widetilde{u}_{Lj}}}(e_i \bar{d}_k)(u_j \widetilde{\chi}^0_1) + \frac{Y_L}{m^2_{\widetilde{\nu}_{Li}}}(d_j \bar{d}_k)(\nu_i \widetilde{\chi}^0_1) - \frac{Y_L}{m^2_{\widetilde{e}_{Li}}}(u_j \bar{d}_k)(e_i \widetilde{\chi}^0_1)\Big] + \text{h.c.}\,. \end{aligned} \tag{C.6}$$

In order to rearrange the currents into pure-quark and lepton-neutralino currents, we apply Fierz identities, assuming the sfermions are mass degenerate $m_{\widetilde{f}} \approx m_{\text{SUSY}}$ and insert the explicit hypercharges

$$\begin{aligned}\mathcal{L} \supset \frac{3\sqrt{2}g'\lambda'_{ijk}}{4m^2_{\text{SUSY}}}\Big\{&(\bar{\widetilde{\chi}}^0_1 e_i)(\bar{d}_k u_j) - (\bar{\widetilde{\chi}}^0_1 \nu_i)(\bar{d}_k d_j) \\ &- \frac{1}{9}(\bar{\widetilde{\chi}}^0_1 \sigma_2^{\mu\nu} e_i)(\bar{d}_k \sigma_{2,\mu\nu} u_j) + \frac{1}{9}(\bar{\widetilde{\chi}}^0_1 \sigma_2^{\mu\nu} \nu_i)(\bar{d}_k \sigma_{2,\mu\nu} d_j)\Big\} + \text{h.c.}\,. \end{aligned} \tag{C.7}$$

To relate the effective interactions in two-component notation to four-component Dirac spinors, we use appendix G of ref. [181]. The final effective interactions in four-component notation in the mass basis (noting that $d^i_L = V^{ij} d^{j,\text{mass}}_L$) are

$$\begin{aligned}\mathcal{L} \supset &\frac{3\sqrt{2}g'\lambda'_{ijk}}{4m^2_{\text{SUSY}}}\Big\{(\bar{\widetilde{\chi}}^0_1 e^i_L)(\bar{d}^k_R u^j_L) - \frac{1}{36}(\bar{\widetilde{\chi}}^0_1 \sigma_4^{\mu\nu} e^i_L)(\bar{d}^k_R \sigma_{4,\mu\nu} u^j_L)\Big\} \\ &+ \frac{3\sqrt{2}g'\lambda'_{ilk}}{4m^2_{\text{SUSY}}}V^{lj}\Big\{-(\bar{\widetilde{\chi}}^0_1 \nu^i_L)(\bar{d}^k_R d^j_L) + \frac{1}{36}(\bar{\widetilde{\chi}}^0_1 \sigma_4^{\mu\nu} \nu^i_L)(\bar{d}^k_R \sigma_{4,\mu\nu} d^j_L)\Big\} + \text{h.c.}\,. \end{aligned} \tag{C.8}$$

JHEP01(2024)108

Open Access. This article is distributed under the terms of the Creative Commons Attribution License (CC-BY4.0), which permits any use, distribution and reproduction in any medium, provided the original author(s) and source are credited.

References

[1] DUNE collaboration, *Deep Underground Neutrino Experiment (DUNE), Far Detector Technical Design Report, Volume I Introduction to DUNE*, 2020 *JINST* **15** T08008 [arXiv:2002.02967] [INSPIRE].

[2] DUNE collaboration, *Deep Underground Neutrino Experiment (DUNE), Far Detector Technical Design Report, Volume II: DUNE Physics*, arXiv:2002.03005 [INSPIRE].

[3] DUNE collaboration, *Long-baseline neutrino oscillation physics potential of the DUNE experiment*, *Eur. Phys. J. C* **80** (2020) 978 [arXiv:2006.16043] [INSPIRE].

[4] DUNE collaboration, *Experiment Simulation Configurations Approximating DUNE TDR*, arXiv:2103.04797 [INSPIRE].

[5] DUNE collaboration, *Low exposure long-baseline neutrino oscillation sensitivity of the DUNE experiment*, *Phys. Rev. D* **105** (2022) 072006 [arXiv:2109.01304] [INSPIRE].

[6] DUNE collaboration, *Long-Baseline Neutrino Facility (LBNF) and Deep Underground Neutrino Experiment (DUNE): Conceptual Design Report, Volume 2: The Physics Program for DUNE at LBNF*, arXiv:1512.06148 [INSPIRE].

[7] J. Alimena et al., *Searching for long-lived particles beyond the Standard Model at the Large Hadron Collider*, *J. Phys. G* **47** (2020) 090501 [arXiv:1903.04497] [INSPIRE].

[8] L. Lee, C. Ohm, A. Soffer and T.-T. Yu, *Collider Searches for Long-Lived Particles Beyond the Standard Model*, *Prog. Part. Nucl. Phys.* **106** (2019) 210 [*Erratum ibid.* **122** (2022) 103912] [arXiv:1810.12602] [INSPIRE].

[9] D. Curtin et al., *Long-Lived Particles at the Energy Frontier: The MATHUSLA Physics Case*, *Rept. Prog. Phys.* **82** (2019) 116201 [arXiv:1806.07396] [INSPIRE].

[10] S. Knapen and S. Lowette, *A guide to hunting long-lived particles at the LHC*, arXiv:2212.03883 [INSPIRE].

[11] DUNE collaboration, *Deep Underground Neutrino Experiment (DUNE) Near Detector Conceptual Design Report*, *Instruments* **5** (2021) 31 [arXiv:2103.13910] [INSPIRE].

[12] B. Batell et al., *Dark Sector Studies with Neutrino Beams*, in the proceedings of the *Snowmass 2021*, Seattle, U.S.A., July 17–26 (2022) [arXiv:2207.06898] [INSPIRE].

[13] M. Costa, R.K. Mishra and S. Verma, *Model agnostic probes of dark sectors at neutrino experiments*, *Phys. Rev. D* **108** (2023) 035041 [arXiv:2211.13253] [INSPIRE].

[14] P.S.B. Dev et al., *Light, long-lived $B-L$ gauge and Higgs bosons at the DUNE near detector*, *JHEP* **07** (2021) 166 [arXiv:2104.07681] [INSPIRE].

[15] R.T. Co, S. Kumar and Z. Liu, *Searches for heavy QCD axions via dimuon final states*, *JHEP* **02** (2023) 111 [arXiv:2210.02462] [INSPIRE].

[16] K.J. Kelly, S. Kumar and Z. Liu, *Heavy axion opportunities at the DUNE near detector*, *Phys. Rev. D* **103** (2021) 095002 [arXiv:2011.05995] [INSPIRE].

[17] I. Krasnov, *DUNE prospects in the search for sterile neutrinos*, *Phys. Rev. D* **100** (2019) 075023 [arXiv:1902.06099] [INSPIRE].

JHEP01(2024)108

[18] P. Ballett, T. Boschi and S. Pascoli, *Heavy Neutral Leptons from low-scale seesaws at the DUNE Near Detector*, *JHEP* **03** (2020) 111 [arXiv:1905.00284] [INSPIRE].

[19] J.M. Berryman et al., *Searches for Decays of New Particles in the DUNE Multi-Purpose Near Detector*, *JHEP* **02** (2020) 174 [arXiv:1912.07622] [INSPIRE].

[20] P. Coloma et al., *GeV-scale neutrinos: interactions with mesons and DUNE sensitivity*, *Eur. Phys. J. C* **81** (2021) 78 [arXiv:2007.03701] [INSPIRE].

[21] M. Ovchynnikov, T. Schwetz and J.-Y. Zhu, *Dipole portal and neutrinophilic scalars at DUNE revisited: The importance of the high-energy neutrino tail*, *Phys. Rev. D* **107** (2023) 055029 [arXiv:2210.13141] [INSPIRE].

[22] DUNE collaboration, *Sensitivity to Heavy Neutral Leptons with the SAND detector at the DUNE ND complex*, arXiv:2209.01899 [INSPIRE].

[23] K.-J. Plows and X. Lu, *Modeling heavy neutral leptons in accelerator beamlines*, *Phys. Rev. D* **107** (2023) 055003 [arXiv:2211.10210] [INSPIRE].

[24] P. Coloma, J. Martín-Albo and S. Urrea, *Discovering Long-lived Particles at DUNE*, arXiv:2309.06492 [INSPIRE].

[25] P. Minkowski, $\mu \to e\gamma$ *at a Rate of One Out of* 10^9 *Muon Decays?*, *Phys. Lett. B* **67** (1977) 421 [INSPIRE].

[26] T. Yanagida, *Horizontal gauge symmetry and masses of neutrinos*, *Conf. Proc. C* **7902131** (1979) 95 [INSPIRE].

[27] M. Gell-Mann, P. Ramond and R. Slansky, *Complex Spinors and Unified Theories*, *Conf. Proc. C* **790927** (1979) 315 [arXiv:1306.4669] [INSPIRE].

[28] R.N. Mohapatra and G. Senjanovic, *Neutrino Mass and Spontaneous Parity Nonconservation*, *Phys. Rev. Lett.* **44** (1980) 912 [INSPIRE].

[29] J. Schechter and J.W.F. Valle, *Neutrino Masses in* $\mathrm{SU}(2) \times \mathrm{U}(1)$ *Theories*, *Phys. Rev. D* **22** (1980) 2227 [INSPIRE].

[30] A. Davidson, $B - L$ *as the fourth color within an* $\mathrm{SU}(2)_L \times \mathrm{U}(1)_R \times \mathrm{U}(1)$ *model*, *Phys. Rev. D* **20** (1979) 776 [INSPIRE].

[31] R.N. Mohapatra and R.E. Marshak, *Local* $B - L$ *Symmetry of Electroweak Interactions, Majorana Neutrinos and Neutron Oscillations*, *Phys. Rev. Lett.* **44** (1980) 1316 [*Erratum ibid.* **44** (1980) 1643] [INSPIRE].

[32] F. Deppisch, S. Kulkarni and W. Liu, *Heavy neutrino production via* Z' *at the lifetime frontier*, *Phys. Rev. D* **100** (2019) 035005 [arXiv:1905.11889] [INSPIRE].

[33] C.-W. Chiang, G. Cottin, A. Das and S. Mandal, *Displaced heavy neutrinos from* Z' *decays at the LHC*, *JHEP* **12** (2019) 070 [arXiv:1908.09838] [INSPIRE].

[34] A. Davidson and K.C. Wali, *Universal Seesaw Mechanism?*, *Phys. Rev. Lett.* **59** (1987) 393 [INSPIRE].

[35] T. Appelquist, B.A. Dobrescu and A.R. Hopper, *Nonexotic Neutral Gauge Bosons*, *Phys. Rev. D* **68** (2003) 035012 [hep-ph/0212073] [INSPIRE].

[36] R.N. Mohapatra and J.C. Pati, *A Natural Left-Right Symmetry*, *Phys. Rev. D* **11** (1975) 2558 [INSPIRE].

[37] J.C. Pati and A. Salam, *Lepton Number as the Fourth Color*, *Phys. Rev. D* **10** (1974) 275 [INSPIRE].

JHEP01(2024)108

[38] R.N. Mohapatra and G. Senjanovic, *Neutrino Masses and Mixings in Gauge Models with Spontaneous Parity Violation*, *Phys. Rev. D* **23** (1981) 165 [INSPIRE].

[39] W.-Y. Keung and G. Senjanovic, *Majorana Neutrinos and the Production of the Right-handed Charged Gauge Boson*, *Phys. Rev. Lett.* **50** (1983) 1427 [INSPIRE].

[40] F. del Aguila, S. Bar-Shalom, A. Soni and J. Wudka, *Heavy Majorana Neutrinos in the Effective Lagrangian Description: Application to Hadron Colliders*, *Phys. Lett. B* **670** (2009) 399 [arXiv:0806.0876] [INSPIRE].

[41] ATLAS collaboration, *Search for doubly charged Higgs boson production in multi-lepton final states with the ATLAS detector using proton-proton collisions at* $\sqrt{s} = 13$ *TeV*, *Eur. Phys. J. C* **78** (2018) 199 [arXiv:1710.09748] [INSPIRE].

[42] Y. Liao and X.-D. Ma, *Operators up to Dimension Seven in Standard Model Effective Field Theory Extended with Sterile Neutrinos*, *Phys. Rev. D* **96** (2017) 015012 [arXiv:1612.04527] [INSPIRE].

[43] M. Chala and A. Titov, *One-loop matching in the SMEFT extended with a sterile neutrino*, *JHEP* **05** (2020) 139 [arXiv:2001.07732] [INSPIRE].

[44] I. Bischer and W. Rodejohann, *General neutrino interactions from an effective field theory perspective*, *Nucl. Phys. B* **947** (2019) 114746 [arXiv:1905.08699] [INSPIRE].

[45] J. De Vries et al., *Long-lived Sterile Neutrinos at the LHC in Effective Field Theory*, *JHEP* **03** (2021) 148 [arXiv:2010.07305] [INSPIRE].

[46] G. Cottin et al., *Heavy neutral leptons in effective field theory and the high-luminosity LHC*, *JHEP* **09** (2021) 039 [arXiv:2105.13851] [INSPIRE].

[47] R. Beltrán et al., *Long-lived heavy neutral leptons at the LHC: four-fermion single-*N_R *operators*, *JHEP* **01** (2022) 044 [arXiv:2110.15096] [INSPIRE].

[48] W. Dekens et al., *Sterile neutrinos and neutrinoless double beta decay in effective field theory*, *JHEP* **06** (2020) 097 [arXiv:2002.07182] [INSPIRE].

[49] G. Zhou, *Light sterile neutrinos and lepton-number-violating kaon decays in effective field theory*, *JHEP* **06** (2022) 127 [arXiv:2112.00767] [INSPIRE].

[50] T. Li, X.-D. Ma and M.A. Schmidt, *General neutrino interactions with sterile neutrinos in light of coherent neutrino-nucleus scattering and meson invisible decays*, *JHEP* **07** (2020) 152 [arXiv:2005.01543] [INSPIRE].

[51] R. Beltrán et al., *Long-lived heavy neutral leptons from mesons in effective field theory*, *JHEP* **01** (2023) 015 [arXiv:2210.02461] [INSPIRE].

[52] R. Beltrán et al., *Reinterpretation of searches for long-lived particles from meson decays*, *JHEP* **05** (2023) 031 [arXiv:2302.03216] [INSPIRE].

[53] R. Beltrán et al., *Heavy neutral leptons from kaons in effective field theory*, arXiv:2309.11546 [INSPIRE].

[54] G. Zhou et al., *Long-lived sterile neutrinos at Belle II in effective field theory*, *JHEP* **04** (2022) 057 [arXiv:2111.04403] [INSPIRE].

[55] T. Han, J. Liao, H. Liu and D. Marfatia, *Right-handed Dirac and Majorana neutrinos at Belle II*, *JHEP* **04** (2023) 013 [*Erratum ibid.* **09** (2023) 016] [arXiv:2207.07029] [INSPIRE].

[56] H.K. Dreiner, *An introduction to explicit R-parity violation*, *Adv. Ser. Direct. High Energy Phys.* **21** (2010) 565 [hep-ph/9707435] [INSPIRE].

JHEP01(2024)108

[57] B.C. Allanach, A. Dedes and H.K. Dreiner, *R parity violating minimal supergravity model*, *Phys. Rev. D* **69** (2004) 115002 [*Erratum ibid.* **72** (2005) 079902] [hep-ph/0309196] [INSPIRE].

[58] R. Barbier et al., *R-parity violating supersymmetry*, *Phys. Rept.* **420** (2005) 1 [hep-ph/0406039] [INSPIRE].

[59] R.N. Mohapatra, *Supersymmetry and R-parity: an Overview*, *Phys. Scripta* **90** (2015) 088004 [arXiv:1503.06478] [INSPIRE].

[60] D. Choudhury, H.K. Dreiner, P. Richardson and S. Sarkar, *A supersymmetric solution to the KARMEN time anomaly*, *Phys. Rev. D* **61** (2000) 095009 [hep-ph/9911365] [INSPIRE].

[61] A. Dedes, H.K. Dreiner and P. Richardson, *Attempts at explaining the NuTeV observation of dimuon events*, *Phys. Rev. D* **65** (2001) 015001 [hep-ph/0106199] [INSPIRE].

[62] I. Gogoladze, J.D. Lykken, C. Macesanu and S. Nandi, *Implications of a Massless Neutralino for Neutrino Physics*, *Phys. Rev. D* **68** (2003) 073004 [hep-ph/0211391] [INSPIRE].

[63] H.K. Dreiner et al., *Mass Bounds on a Very Light Neutralino*, *Eur. Phys. J. C* **62** (2009) 547 [arXiv:0901.3485] [INSPIRE].

[64] F. Domingo and H.K. Dreiner, *Decays of a bino-like particle in the low-mass regime*, *SciPost Phys.* **14** (2023) 134 [arXiv:2205.08141] [INSPIRE].

[65] J.A. Grifols, E. Masso and S. Peris, *Photinos From Gravitational Collapse*, *Phys. Lett. B* **220** (1989) 591 [INSPIRE].

[66] J.R. Ellis, K.A. Olive, S. Sarkar and D.W. Sciama, *Low Mass Photinos and Supernova SN1987A*, *Phys. Lett. B* **215** (1988) 404 [INSPIRE].

[67] K. Lau, *Constraints on supersymmetry from SN1987A*, *Phys. Rev. D* **47** (1993) 1087 [INSPIRE].

[68] H.K. Dreiner, C. Hanhart, U. Langenfeld and D.R. Phillips, *Supernovae and light neutralinos: SN1987A bounds on supersymmetry revisited*, *Phys. Rev. D* **68** (2003) 055004 [hep-ph/0304289] [INSPIRE].

[69] H.K. Dreiner, J.-F. Fortin, J. Isern and L. Ubaldi, *White Dwarfs constrain Dark Forces*, *Phys. Rev. D* **88** (2013) 043517 [arXiv:1303.7232] [INSPIRE].

[70] S. Profumo, *Hunting the lightest lightest neutralinos*, *Phys. Rev. D* **78** (2008) 023507 [arXiv:0806.2150] [INSPIRE].

[71] H.K. Dreiner, M. Hanussek, J.S. Kim and S. Sarkar, *Gravitino cosmology with a very light neutralino*, *Phys. Rev. D* **85** (2012) 065027 [arXiv:1111.5715] [INSPIRE].

[72] H.K. Dreiner et al., *Recasting bounds on long-lived heavy neutral leptons in terms of a light supersymmetric R-parity violating neutralino*, *JHEP* **08** (2023) 058 [arXiv:2306.14700] [INSPIRE].

[73] E.J. Chun and H.B. Kim, *Nonthermal axino as cool dark matter in supersymmetric standard model without R-parity*, *Phys. Rev. D* **60** (1999) 095006 [hep-ph/9906392] [INSPIRE].

[74] G. Belanger, F. Boudjema, A. Pukhov and S. Rosier-Lees, *A lower limit on the neutralino mass in the MSSM with nonuniversal gaugino masses*, in the proceedings of the *10th International Conference on Supersymmetry and Unification of Fundamental Interactions (SUSY02)*, Hamburg, Germany, June 17–23 (2002), p. 919–924 [hep-ph/0212227] [INSPIRE].

[75] D. Hooper and T. Plehn, *Supersymmetric dark matter: How light can the LSP be?*, *Phys. Lett. B* **562** (2003) 18 [hep-ph/0212226] [INSPIRE].

JHEP01(2024)108

[76] A. Bottino, N. Fornengo and S. Scopel, *Light relic neutralinos*, *Phys. Rev. D* **67** (2003) 063519 [hep-ph/0212379] [INSPIRE].

[77] G. Belanger et al., *Lower limit on the neutralino mass in the general MSSM*, *JHEP* **03** (2004) 012 [hep-ph/0310037] [INSPIRE].

[78] D. Albornoz Vasquez et al., *Can neutralinos in the MSSM and NMSSM scenarios still be light?*, *Phys. Rev. D* **82** (2010) 115027 [arXiv:1009.4380] [INSPIRE].

[79] L. Calibbi, J.M. Lindert, T. Ota and Y. Takanishi, *Cornering light Neutralino Dark Matter at the LHC*, *JHEP* **10** (2013) 132 [arXiv:1307.4119] [INSPIRE].

[80] S. Colucci, H.K. Dreiner and L. Ubaldi, *Supersymmetric R -parity violating Dine-Fischler-Srednicki-Zhitnitsky axion model*, *Phys. Rev. D* **99** (2019) 015003 [arXiv:1807.02530] [INSPIRE].

[81] P. Bechtle et al., *Killing the cMSSM softly*, *Eur. Phys. J. C* **76** (2016) 96 [arXiv:1508.05951] [INSPIRE].

[82] H.K. Dreiner, G. Polesello and M. Thormeier, *Bounds on broken R parity from leptonic meson decays*, *Phys. Rev. D* **65** (2002) 115006 [hep-ph/0112228] [INSPIRE].

[83] H. Dreiner, G. Polesello and M. Thormeier, *Bounds on broken R parity from NOMAD and CHORUS*, hep-ph/0207160 [INSPIRE].

[84] H.K. Dreiner et al., *Rare meson decays into very light neutralinos*, *Phys. Rev. D* **80** (2009) 035018 [arXiv:0905.2051] [INSPIRE].

[85] D. Dercks et al., *R-Parity Violation at the LHC*, *Eur. Phys. J. C* **77** (2017) 856 [arXiv:1706.09418] [INSPIRE].

[86] ATLAS collaboration, *Search for photonic signatures of gauge-mediated supersymmetry in* 13 *TeV pp collisions with the ATLAS detector*, *Phys. Rev. D* **97** (2018) 092006 [arXiv:1802.03158] [INSPIRE].

[87] CMS collaboration, *Search for gauge-mediated supersymmetry in events with at least one photon and missing transverse momentum in pp collisions at* $\sqrt{s} = 13$ *TeV*, *Phys. Lett. B* **780** (2018) 118 [arXiv:1711.08008] [INSPIRE].

[88] CMS collaboration, *Search for supersymmetry in final states with photons and missing transverse momentum in proton-proton collisions at* 13 *TeV*, *JHEP* **06** (2019) 143 [arXiv:1903.07070] [INSPIRE].

[89] CMS collaboration, *Search for supersymmetry in proton-proton collisions at* 13 *TeV in final states with jets and missing transverse momentum*, *JHEP* **10** (2019) 244 [arXiv:1908.04722] [INSPIRE].

[90] ATLAS collaboration, *Search for new phenomena in final states with large jet multiplicities and missing transverse momentum using* $\sqrt{s} = 13$ *TeV proton-proton collisions recorded by ATLAS in Run 2 of the LHC*, *JHEP* **10** (2020) 062 [arXiv:2008.06032] [INSPIRE].

[91] H.K. Dreiner et al., *The ABC of RPV: classification of R-parity violating signatures at the LHC for small couplings*, *JHEP* **07** (2023) 215 [arXiv:2306.07317] [INSPIRE].

[92] J. de Vries, H.K. Dreiner and D. Schmeier, *R-Parity Violation and Light Neutralinos at SHiP and the LHC*, *Phys. Rev. D* **94** (2016) 035006 [arXiv:1511.07436] [INSPIRE].

[93] G. Cottin et al., *Searching for light neutralinos with a displaced vertex at the LHC*, *JHEP* **10** (2022) 095 [arXiv:2208.12818] [INSPIRE].

JHEP01(2024)108

[94] Z.S. Wang and K. Wang, *Long-lived light neutralinos at future Z-factories*, *Phys. Rev. D* **101** (2020) 115018 [arXiv:1904.10661] [INSPIRE].

[95] D. Dercks, J. De Vries, H.K. Dreiner and Z.S. Wang, *R-parity Violation and Light Neutralinos at CODEX-b, FASER, and MATHUSLA*, *Phys. Rev. D* **99** (2019) 055039 [arXiv:1810.03617] [INSPIRE].

[96] D. Dercks, H.K. Dreiner, M. Hirsch and Z.S. Wang, *Long-Lived Fermions at AL3X*, *Phys. Rev. D* **99** (2019) 055020 [arXiv:1811.01995] [INSPIRE].

[97] H.K. Dreiner, J.Y. Günther and Z.S. Wang, *R-parity violation and light neutralinos at ANUBIS and MAPP*, *Phys. Rev. D* **103** (2021) 075013 [arXiv:2008.07539] [INSPIRE].

[98] H.K. Dreiner, D. Köhler, S. Nangia and Z.S. Wang, *Searching for a single photon from lightest neutralino decays in R-parity-violating supersymmetry at FASER*, *JHEP* **02** (2023) 120 [arXiv:2207.05100] [INSPIRE].

[99] SHiP collaboration, *A facility to Search for Hidden Particles (SHiP) at the CERN SPS*, arXiv:1504.04956 [INSPIRE].

[100] S. Dey et al., *Long-lived light neutralinos at Belle II*, *JHEP* **02** (2021) 211 [arXiv:2012.00438] [INSPIRE].

[101] C.O. Dib et al., *Probing R-parity violation in B-meson decays to a baryon and a light neutralino*, *JHEP* **02** (2023) 224 [arXiv:2208.06421] [INSPIRE].

[102] P. Candia, G. Cottin, A. Méndez and V. Muñoz, *Searching for light long-lived neutralinos at Super-Kamiokande*, *Phys. Rev. D* **104** (2021) 055024 [arXiv:2107.02804] [INSPIRE].

[103] J.M. Butterworth et al., *Higgs phenomenology as a probe of sterile neutrinos*, *Phys. Rev. D* **100** (2019) 115019 [arXiv:1909.04665] [INSPIRE].

[104] B.C. Canas et al., *Updating neutrino magnetic moment constraints*, *Phys. Lett. B* **753** (2016) 191 [arXiv:1510.01684] [INSPIRE].

[105] D. Barducci, E. Bertuzzo, M. Taoso and C. Toni, *Probing right-handed neutrinos dipole operators*, *JHEP* **03** (2023) 239 [arXiv:2209.13469] [INSPIRE].

[106] W. Liu and Y. Zhang, *Testing neutrino dipole portal by long-lived particle detectors at the LHC*, *Eur. Phys. J. C* **83** (2023) 568 [arXiv:2302.02081] [INSPIRE].

[107] D. Barducci et al., *Probing the dipole portal to heavy neutral leptons via meson decays at the high-luminosity LHC*, *Phys. Rev. D* **108** (2023) 115009 [arXiv:2308.16608] [INSPIRE].

[108] Y. Liao, X.-D. Ma and H.-L. Wang, *Effective field theory approach to lepton number violating decays $K^{\pm} \to \pi^{\mp} l_{\alpha}^{\pm} l_{\beta}^{\pm}$: long-distance contribution*, *JHEP* **03** (2020) 120 [arXiv:2001.07378] [INSPIRE].

[109] W. Buchmuller, R. Ruckl and D. Wyler, *Leptoquarks in Lepton-Quark Collisions*, *Phys. Lett. B* **191** (1987) 442 [INSPIRE].

[110] I. Doršner et al., *Physics of leptoquarks in precision experiments and at particle colliders*, *Phys. Rept.* **641** (2016) 1 [arXiv:1603.04993] [INSPIRE].

[111] Particle Data Group collaboration, *Review of Particle Physics*, *PTEP* **2022** (2022) 083C01 [INSPIRE].

[112] ATLAS collaboration, *Search for new resonances in mass distributions of jet pairs using 139 fb^{-1} of pp collisions at $\sqrt{s} = 13$ TeV with the ATLAS detector*, *JHEP* **03** (2020) 145 [arXiv:1910.08447] [INSPIRE].

JHEP01(2024)108

[113] W. Dekens et al., *A low-energy perspective on the minimal left-right symmetric model*, *JHEP* **11** (2021) 127 [arXiv:2107.10852] [INSPIRE].

[114] G.F.S. Alves, C.S. Fong, L.P.S. Leal and R. Zukanovich Funchal, *New limits on W_R from meson decays*, arXiv:2307.04862 [INSPIRE].

[115] H.K. Dreiner, H.E. Haber and S.P. Martin, *From Spinors to Supersymmetry*, Cambridge University Press, Cambridge, U.K. (2023) [DOI:10.1017/9781139049740] [INSPIRE].

[116] J.C. Helo, M. Hirsch and Z.S. Wang, *Heavy neutral fermions at the high-luminosity LHC*, *JHEP* **07** (2018) 056 [arXiv:1803.02212] [INSPIRE].

[117] M. Hirsch and Z.S. Wang, *Heavy neutral leptons at ANUBIS*, *Phys. Rev. D* **101** (2020) 055034 [arXiv:2001.04750] [INSPIRE].

[118] M. Fieg, F. Kling, H. Schulz and T. Sjöstrand, *Tuning Pythia for Forward Physics Experiments*, arXiv:2309.08604 [INSPIRE].

[119] I. Boiarska et al., *Phenomenology of GeV-scale scalar portal*, *JHEP* **11** (2019) 162 [arXiv:1904.10447] [INSPIRE].

[120] K. Bondarenko, A. Boyarsky, D. Gorbunov and O. Ruchayskiy, *Phenomenology of GeV-scale Heavy Neutral Leptons*, *JHEP* **11** (2018) 032 [arXiv:1805.08567] [INSPIRE].

[121] L.M. Johnson, D.W. McKay and T. Bolton, *Extending sensitivity for low mass neutral heavy lepton searches*, *Phys. Rev. D* **56** (1997) 2970 [hep-ph/9703333] [INSPIRE].

[122] V. Gribanov, S. Kovalenko and I. Schmidt, *Sterile neutrinos in tau lepton decays*, *Nucl. Phys. B* **607** (2001) 355 [hep-ph/0102155] [INSPIRE].

[123] D. Gorbunov and M. Shaposhnikov, *How to find neutral leptons of the νMSM?*, *JHEP* **10** (2007) 015 [*Erratum ibid.* **11** (2013) 101] [arXiv:0705.1729] [INSPIRE].

[124] A. Atre, T. Han, S. Pascoli and B. Zhang, *The Search for Heavy Majorana Neutrinos*, *JHEP* **05** (2009) 030 [arXiv:0901.3589] [INSPIRE].

[125] S.G. Gorishnii, A.L. Kataev and S.A. Larin, *The three loop QED contributions to the photon vacuum polarization function in the MS scheme and the four loop corrections to the QED beta function in the on-shell scheme*, *Phys. Lett. B* **273** (1991) 141 [*Erratum ibid.* **275** (1992) 512] [INSPIRE].

[126] J.C. Helo, S. Kovalenko and I. Schmidt, *Sterile neutrinos in lepton number and lepton flavor violating decays*, *Nucl. Phys. B* **853** (2011) 80 [arXiv:1005.1607] [INSPIRE].

[127] DUNE collaboration, *Long-Baseline Neutrino Facility (LBNF) and Deep Underground Neutrino Experiment (DUNE): Conceptual Design Report, Volume 1: The LBNF and DUNE Projects*, arXiv:1601.05471 [INSPIRE].

[128] DUNE collaboration, *Long-Baseline Neutrino Facility (LBNF) and Deep Underground Neutrino Experiment (DUNE): Conceptual Design Report, Volume 3: Long-Baseline Neutrino Facility for DUNE June 24, 2015*, arXiv:1601.05823 [INSPIRE].

[129] DUNE collaboration, *Long-Baseline Neutrino Facility (LBNF) and Deep Underground Neutrino Experiment (DUNE): Conceptual Design Report, Volume 4 The DUNE Detectors at LBNF*, arXiv:1601.02984 [INSPIRE].

[130] C. Lourenco and H.K. Wohri, *Heavy flavour hadro-production from fixed-target to collider energies*, *Phys. Rept.* **433** (2006) 127 [hep-ph/0609101] [INSPIRE].

[131] B. Andersson, G. Gustafson, G. Ingelman and T. Sjöstrand, *Parton Fragmentation and String Dynamics*, *Phys. Rept.* **97** (1983) 31 [INSPIRE].

JHEP01(2024)108

[132] SHiP collaboration, *Sensitivity of the SHiP experiment to Heavy Neutral Leptons*, *JHEP* **04** (2019) 077 [arXiv:1811.00930] [INSPIRE].

[133] Particle Data Group collaboration, *Review of Particle Physics*, *Phys. Rev. D* **98** (2018) 030001 [INSPIRE].

[134] C. Bierlich et al., *A comprehensive guide to the physics and usage of PYTHIA 8.3*, *SciPost Phys. Codeb.* **2022** (2022) 8 [arXiv:2203.11601] [INSPIRE].

[135] T. Sjöstrand et al., *An introduction to PYTHIA 8.2*, *Comput. Phys. Commun.* **191** (2015) 159 [arXiv:1410.3012] [INSPIRE].

[136] J.L. Feng, I. Galon, F. Kling and S. Trojanowski, *ForwArd Search ExpeRiment at the LHC*, *Phys. Rev. D* **97** (2018) 035001 [arXiv:1708.09389] [INSPIRE].

[137] FASER collaboration, *FASER's physics reach for long-lived particles*, *Phys. Rev. D* **99** (2019) 095011 [arXiv:1811.12522] [INSPIRE].

[138] J.L. Feng et al., *The Forward Physics Facility at the High-Luminosity LHC*, *J. Phys. G* **50** (2023) 030501 [arXiv:2203.05090] [INSPIRE].

[139] J.P. Chou, D. Curtin and H.J. Lubatti, *New Detectors to Explore the Lifetime Frontier*, *Phys. Lett. B* **767** (2017) 29 [arXiv:1606.06298] [INSPIRE].

[140] MATHUSLA collaboration, *An update to the Letter of Intent for MATHUSLA: Search for Long-Lived Particles at the HL-LHC*, arXiv:2009.01693 [INSPIRE].

[141] T. Pierog et al., *EPOS LHC: Test of collective hadronization with data measured at the CERN Large Hadron Collider*, *Phys. Rev. C* **92** (2015) 034906 [arXiv:1306.0121] [INSPIRE].

[142] C. Baus, T. Pierog and R. Ulrich, *Cosmic Ray Monte Carlo (CRMC)*, https://gitlab.iap.kit.edu/AirShowerPhysics/crmc.

[143] CMS collaboration, *The CMS Experiment at the CERN LHC*, 2008 *JINST* **3** S08004 [INSPIRE].

[144] ATLAS collaboration, *Technical Design Report for the Phase-II Upgrade of the ATLAS Tile Calorimeter*, CERN-LHCC-2017-019 (2017).

[145] D.M. Gingrich et al., *Construction, assembly and testing of the ATLAS hadronic end-cap calorimeter*, 2007 *JINST* **2** P05005 [INSPIRE].

[146] M. Bauer, O. Brandt, L. Lee and C. Ohm, *ANUBIS: Proposal to search for long-lived neutral particles in CERN service shafts*, arXiv:1909.13022 [INSPIRE].

[147] S. Cerci et al., *FACET: A new long-lived particle detector in the very forward region of the CMS experiment*, *JHEP* **06** (2022) 110 [arXiv:2201.00019] [INSPIRE].

[148] O.S. Bruning et al., *LHC Design Report Vol.1: The LHC Main Ring*, CERN-2004-003-V1 (2004) [DOI:10.5170/CERN-2004-003-V-1].

[149] FASER collaboration, *FASER: ForwArd Search ExpeRiment at the LHC*, arXiv:1901.04468 [INSPIRE].

[150] V.V. Gligorov, S. Knapen, M. Papucci and D.J. Robinson, *Searching for Long-lived Particles: A Compact Detector for Exotics at LHCb*, *Phys. Rev. D* **97** (2018) 015023 [arXiv:1708.09395] [INSPIRE].

[151] J.L. Pinfold, *The MoEDAL Experiment at the LHC — A Progress Report*, *Universe* **5** (2019) 47 [INSPIRE].

[152] J.L. Pinfold, *The MoEDAL experiment: a new light on the high-energy frontier*, *Phil. Trans. Roy. Soc. Lond. A* **377** (2019) 20190382 [INSPIRE].

JHEP01(2024)108

[153] L. Canetti and M. Shaposhnikov, *Baryon Asymmetry of the Universe in the NuMSM*, *JCAP* **09** (2010) 001 [arXiv:1006.0133] [INSPIRE].

[154] PLANCK collaboration, *Planck 2018 results. VI. Cosmological parameters*, *Astron. Astrophys.* **641** (2020) A6 [*Erratum ibid.* **652** (2021) C4] [arXiv:1807.06209] [INSPIRE].

[155] E. Fernández-Martínez et al., *Effective portals to heavy neutral leptons*, *JHEP* **09** (2023) 001 [arXiv:2304.06772] [INSPIRE].

[156] PIENU collaboration, *Improved search for heavy neutrinos in the decay $\pi \to e\nu$*, *Phys. Rev. D* **97** (2018) 072012 [arXiv:1712.03275] [INSPIRE].

[157] D.A. Bryman and R. Shrock, *Constraints on Sterile Neutrinos in the MeV to GeV Mass Range*, *Phys. Rev. D* **100** (2019) 073011 [arXiv:1909.11198] [INSPIRE].

[158] NA62 collaboration, *Search for heavy neutral lepton production in K^+ decays to positrons*, *Phys. Lett. B* **807** (2020) 135599 [arXiv:2005.09575] [INSPIRE].

[159] T2K collaboration, *Search for heavy neutrinos with the T2K near detector ND280*, *Phys. Rev. D* **100** (2019) 052006 [arXiv:1902.07598] [INSPIRE].

[160] R. Barouki, G. Marocco and S. Sarkar, *Blast from the past II: Constraints on heavy neutral leptons from the BEBC WA66 beam dump experiment*, *SciPost Phys.* **13** (2022) 118 [arXiv:2208.00416] [INSPIRE].

[161] DELPHI collaboration, *Search for neutral heavy leptons produced in Z decays*, *Z. Phys. C* **74** (1997) 57 [*Erratum ibid.* **75** (1997) 580] [INSPIRE].

[162] N. Sabti, A. Magalich and A. Filimonova, *An Extended Analysis of Heavy Neutral Leptons during Big Bang Nucleosynthesis*, *JCAP* **11** (2020) 056 [arXiv:2006.07387] [INSPIRE].

[163] H. Leutwyler, *On the $1/N$ expansion in chiral perturbation theory*, *Nucl. Phys. B Proc. Suppl.* **64** (1998) 223 [hep-ph/9709408] [INSPIRE].

[164] T. Feldmann, P. Kroll and B. Stech, *Mixing and decay constants of pseudoscalar mesons*, *Phys. Rev. D* **58** (1998) 114006 [hep-ph/9802409] [INSPIRE].

[165] ETM collaboration, *Tensor form factor of $D \to \pi(K)\ell\nu$ and $D \to \pi(K)\ell\ell$ decays with $N_f = 2+1+1$ twisted-mass fermions*, *Phys. Rev. D* **98** (2018) 014516 [arXiv:1803.04807] [INSPIRE].

[166] FLAVOUR LATTICE AVERAGING GROUP collaboration, *FLAG Review 2019: Flavour Lattice Averaging Group (FLAG)*, *Eur. Phys. J. C* **80** (2020) 113 [arXiv:1902.08191] [INSPIRE].

[167] D. Melikhov and B. Stech, *Weak form-factors for heavy meson decays: An Update*, *Phys. Rev. D* **62** (2000) 014006 [hep-ph/0001113] [INSPIRE].

[168] FLAVOUR LATTICE AVERAGING GROUP (FLAG) collaboration, *FLAG Review 2021*, *Eur. Phys. J. C* **82** (2022) 869 [arXiv:2111.09849] [INSPIRE].

[169] H.K. Dreiner, M. Kramer and B. O'Leary, *Bounds on R-parity violating supersymmetric couplings from leptonic and semi-leptonic meson decays*, *Phys. Rev. D* **75** (2007) 114016 [hep-ph/0612278] [INSPIRE].

[170] M. Neubert and B. Stech, *Nonleptonic weak decays of B mesons*, *Adv. Ser. Direct. High Energy Phys.* **15** (1998) 294 [hep-ph/9705292] [INSPIRE].

[171] D. Bečirević et al., *Lattice QCD and QCD sum rule determination of the decay constants of η_c, J/ψ and h_c states*, *Nucl. Phys. B* **883** (2014) 306 [arXiv:1312.2858] [INSPIRE].

JHEP01(2024)108

[172] I. Baum et al., *Matrix elements of the electromagnetic operator between kaon and pion states*, *Phys. Rev. D* **84** (2011) 074503 [arXiv:1108.1021] [INSPIRE].

[173] NA48 collaboration, *Measurement of $K^0_{\mu 3}$ form factors*, *Phys. Lett. B* **647** (2007) 341 [hep-ex/0703002] [INSPIRE].

[174] O.P. Yushchenko et al., *High statistic study of the $K^- \to \pi^0 \mu^- \nu$ decay*, *Phys. Lett. B* **581** (2004) 31 [hep-ex/0312004] [INSPIRE].

[175] ETM collaboration, *Scalar and vector form factors of $D \to \pi(K)\ell\nu$ decays with $N_f = 2+1+1$ twisted fermions*, *Phys. Rev. D* **96** (2017) 054514 [*Erratum ibid.* **99** (2019) 099902] [arXiv:1706.03017] [INSPIRE].

[176] N.R. Soni et al., *Semileptonic $D_{(s)}$-meson decays in the light of recent data*, *Phys. Rev. D* **98** (2018) 114031 [arXiv:1810.11907] [INSPIRE].

[177] D. Du et al., *Phenomenology of semileptonic B-meson decays with form factors from lattice QCD*, *Phys. Rev. D* **93** (2016) 034005 [arXiv:1510.02349] [INSPIRE].

[178] E. McLean, C.T.H. Davies, J. Koponen and A.T. Lytle, *$B_s \to D_s \ell\nu$ Form Factors for the full q^2 range from Lattice QCD with non-perturbatively normalized currents*, *Phys. Rev. D* **101** (2020) 074513 [arXiv:1906.00701] [INSPIRE].

[179] Fermilab Lattice and MILC collaborations, *$B \to \pi\ell\ell$ form factors for new-physics searches from lattice QCD*, *Phys. Rev. Lett.* **115** (2015) 152002 [arXiv:1507.01618] [INSPIRE].

[180] S.P. Martin, *A Supersymmetry primer*, *Adv. Ser. Direct. High Energy Phys.* **18** (1998) 1 [hep-ph/9709356] [INSPIRE].

[181] H.K. Dreiner, H.E. Haber and S.P. Martin, *Two-component spinor techniques and Feynman rules for quantum field theory and supersymmetry*, *Phys. Rept.* **494** (2010) 1 [arXiv:0812.1594] [INSPIRE].

[182] M. Drees, R. Godbole and P. Roy, *Theory and phenomenology of sparticles: An account of four-dimensional $N = 1$ supersymmetry in high energy physics*, World Scientific (2005) [DOI:10.1142/4001].

[183] H.K. Dreiner, M. Hanussek and C. Luhn, *What is the discrete gauge symmetry of the R-parity violating MSSM?*, *Phys. Rev. D* **86** (2012) 055012 [arXiv:1206.6305] [INSPIRE].

JHEP01(2024)108